

DISSERTATION

Simulation of core level spectra using Density Funcional Theory

ausgeführt zum Zwecke der Erlangung des akademischen Grades eines Doktors der
technischen Wissenschaften unter der Leitung von

Univ. Prof. Dr. phil. Karlheinz Schwarz
E 165
Institut für Materialchemie

eingereicht an der Technischen Universität Wien
Fakultät für Technische Chemie

von

Dipl. Ing. Joachim Luitz
8626200
Wohlmuthgasse 18
A-3003 Gablitz

Wien, am 19. Mai 2006

Kurzfassung

DISSERTATION

Simulation of core level spectra using Density Funcional Theory

von

Dipl. Ing. Joachim Luitz

8626200

In der vorliegenden Arbeit werden zunächst die theoretischen Grundlagen erläutert, die notwendig sind um ausgehend von einer Kristallstruktur einer Substanz deren elektronischen Eigenschaften auf der Basis der Dichtefunktionaltheorie zu berechnen. Daran anschliessend wird der Formalismus zur Berechnung von Elektronen Energie Verlustspektren (Electron Energy Loss Spectra, EELS) dargestellt.

Der zweite Teil dieser Arbeit beschäftigt sich mit der Simulation von einigen ausgewählten Substanzen, von denen EELS berechnet und mit experimentellen Daten verglichen werden. Dabei wurden folgende Substanzen gewählt: Magnesium und Magnesiumoxid, Aluminium und Aluminiumoxid, Titan und Titanoxid sowie Kupfer und Kupferoxid. Diese Kombinationen Metall/Metalloxid wurden mit Bedacht gewählt um die unterschiedlich notwendige Behandlung von Metall und Oxid in der Simulation zu verdeutlichen.

Bei den durchgeführten Simulationen wurde festgestellt, dass die Verwendung eines zumindest partiellen "core hole" (einer elektronischen Fehlstelle in einem Rumpfungszustand) in der Simulation notwendig ist um die Übereinstimmung von Simulation und Experiment zu verbessern.

Für Metalle lässt sich generell sagen, daß ein partielles "core hole" von etwa 0.4 – 0.5 (wobei ein halbes "core hole" dem Slater'schen Übergangszustand entspricht) in den meisten Fällen die Simulation wesentlich verbessert.

Für die Oxide lässt sich feststellen, dass ein "core hole" alleine zu keiner Verbesserung führt, weil keine freien Elektronen zur Verfügung stehen um diese Ladung abzuschirmen. Deshalb sollte die Simulation in einer Superzelle durchgeführt werden um eine künstliche "core hole – core hole" Wechselwirkung zu vermeiden.

Contents

Methods	7
1 Methods	8
1.1 Solid State Theory	8
1.1.1 Introduction	8
1.1.2 The ideal single crystal	9
1.1.3 The Bloch Theorem	9
1.1.4 Born-Oppenheimer approximation	11
1.2 Density Functional Theory	12
1.2.1 Introduction	12
1.2.2 Local Density Approximation	13
1.2.3 Generalized Gradient Approximation	14
1.2.4 The Kohn-Sham equations	14
1.3 The Variational Principle	14
1.4 The "Self Consistent Field (SCF)"	15
1.5 LAPW	16
1.5.1 Introduction	16
1.5.2 Basis Set in the LAPW method	16
1.5.3 Solving the Schrödinger equation	18
1.5.4 The electron density	18
1.5.5 The potential and total energy	19
1.5.6 Description of electronic states	20
1.5.7 Summation of states	21
1.6 The APW+lo method	21

<i>CONTENTS</i>	4
1.7 Simulating Spectra	22
1.7.1 Introduction	22
1.7.2 Inelastic scattering	23
1.7.3 ELNES	24
1.7.4 The Dynamic Form Factor	24
1.7.5 Near Edge electron energy loss spectra (ELNES)	27
1.7.6 TELNES.2 - new development	29
1.7.7 X-ray emission and absorption spectra (XES, XAS)	34
1.8 Broadening of spectra	35
1.8.1 Broadening of the core state	35
1.8.2 Broadening of valence states	35
1.8.3 Instrumental broadening	37
1.9 The Core Hole	37
1.9.1 Initial State Approximation	37
1.9.2 Final State Approximation	37
1.9.3 Partial Core Hole Screening (PCS)	38
1.9.4 Slater's Transition State	38
1.9.5 Beyond these simple concepts	38
Programs	39
2 Programs	40
2.1 WIEN2k	40
2.1.1 Introduction	40
2.1.2 Input	40
2.1.3 Initialization	41
2.1.4 SCF cycle	41
2.2 XSPEC	43
2.3 ELNES	43
2.4 TELNES.2	44
2.5 BROADENING	45

<i>CONTENTS</i>	5
Results	47
3 Results	48
3.1 Aluminum	49
3.1.1 Aluminum metal	49
3.1.2 Aluminum oxide	51
3.2 Magnesium	53
3.2.1 Magnesium metal	53
3.2.2 Magnesium oxide	54
3.3 Titanium	57
3.3.1 Titanium metal	57
3.3.2 Titanium oxide	59
3.4 Copper	61
3.4.1 Copper metal	61
3.4.2 Copper oxide	64
Conclusion	67
4 Conclusion	68
Thanks	69
Bibliography	70
Curriculum Vitae	76

Foreword

I have started this thesis many years ago and should have written it 4-5 years ago. I did not write it then, because there were so many projects in my life that were more appealing to me. Bits and pieces of what is presented here have already been published and disseminated in various other ways: articles, posters and (invited) talks, despite the fact that I have left University in 2001.

However, today, I believe it is high time that I summarize this work in order to finish my long term project called "PhD thesis".

Methods

*Physics is like sex.
Sure, it may give some practical results,
but that's not why we do it.*
Richard Feynman

1 Methods

1.1 Solid State Theory

1.1.1 Introduction

There are two principal types of solids, amorphous and crystalline matter. In amorphous solids some sort of local ordering can be observed. However, there is no periodicity which is typical for crystals, where interactions over long ranges are present. For ideal crystals this periodicity allows to reduce the problem of an infinite body to the calculation of a smaller, but finite number of atoms [24].

For the calculation of quantitative properties of solids, we utilise the time-independent Schrödinger equation:

$$H\Psi = E\Psi \tag{1.1}$$

In this equation Ψ is the crystal wave function, E the energy eigenvalues and H the Hamilton operator. The Hamiltonian in Rydberg atomic units is given by:

$$H = (-\nabla^2 + V) \tag{1.2}$$

where ∇ stands for the Nabla operator and V the potential which is split into components as described later (see 1.2).

The Schrödinger equation can be solved exactly only for one-electron systems. When extending the problem to more electrons, approximations are required. Further when we look at solids, which are in principle infinite in three dimensions, and thus include atoms in the order of 10^{23} even in a small volume, we must rely on methods to reduce this problem.

In the following sections I will describe which assumptions and which concepts are necessary to solve the Schrödinger equation for an infinite solid.

1.1.2 The ideal single crystal

The ideal single crystal is defined by a structure that is infinite in three dimensions, has a fixed, given composition and a rigid translational symmetry.

From this idealisation follows, that inhomogeneities such as surfaces or interfaces are not allowed. However, later I will show how such problems can be tackled, even under the assumption of a 3-dimensional infinite crystal.

Most calculations in solid state science are described in reciprocal space. The lattice vectors in reciprocal space are chosen such that they are orthogonal to those of the lattice in real space:

$$\vec{a}_i \vec{b}_j = 2\pi \delta_{ij} \quad (1.3)$$

The unit cell in reciprocal space is the so called “first Brillouin zone”. Instead of describing this unit cells as parallelepipeds, we can find several types of polyhedra with which we can fill space by translation. A very important type of space filling is obtained by the *Dirichlet construction*. Each lattice point is connected to its nearest neighbours and the corresponding bisection (perpendicular) planes will delimit a region of space which is called the Brillouin zone. This cell is uniquely defined and has additional symmetry properties.

The construction of such a cell can also done in real space and is called “Wigner-Seitz Cell”.

1.1.3 The Bloch Theorem

The calculation of properties of a solid would not be feasible, because all particles contained in the system would have to be considered. In a mole there are $6,023 \cdot 10^{23}$ atoms and all particles (electrons and nuclei) interact with each other. This would result in equations that can never be solved within a finite time.

However, in an ideal single crystal, the infinite problem can be reduced to a small number of atoms due to translation symmetry. Now we can consider solving the resulting problem.

According to Bloch's theorem a crystal wave function can be constructed from a plane wave $e^{i\vec{k}\vec{r}}$ with the wave vector \vec{k} (in reciprocal space) and a function that is periodic in the lattice:

$$\Psi(\vec{r}) = e^{i\vec{k}\vec{r}} u(\vec{r}) \quad (1.4)$$

$$u(\vec{r} + \vec{R}) = u(\vec{r}) \quad (1.5)$$

where \vec{R} is the lattice vector in real space.

Although observable quantities like the electron density (given by $\Psi^*\Psi$) and other physical properties are periodic with respect to the lattice, the wave function Ψ itself is not. We can apply the Bloch theorem to the wave function Ψ and get

$$\Psi(\vec{r} + \vec{a}_i) = e^{i\vec{k}\vec{a}_i}\Psi(\vec{r}) \quad (1.6)$$

where the vectors \vec{a}_i are the base vectors of the lattice.

As we assumed an ideal single crystal without surface, we have to introduce periodic boundary conditions, i.e. we require the wave function to be periodic after N unit cells.

$$\Psi(\vec{r} + N_i\vec{a}_i) = \Psi(\vec{r}) \quad (1.7)$$

$$\Psi(\vec{r} + N_i\vec{a}_i) = e^{i\vec{k}N_i\vec{a}_i}e^{i\vec{k}\vec{r}}u(\vec{r}) \quad i = 1 \dots 3 \quad (1.8)$$

where N is an arbitrarily chosen big integer.

From these equations we derive the following conditions:

$$e^{i\vec{k}N_i\vec{a}_i} = 1 \quad (1.9)$$

$$k_i N_i a_i = 2\pi m \quad m \in N \quad (1.10)$$

$$k_i = m \frac{2\pi}{a_i} \frac{1}{N_i} \quad i = 1 \dots 3 \quad (1.11)$$

Because we defined N_i as a large integer it follows that \vec{k} must be quasi-continuous. It can be proven that $\Psi_{\vec{k}}$ is periodic in reciprocal space.

For a complete lattice vector \vec{K} in reciprocal space the following equation holds:

$$\Psi_{\vec{k}}(\vec{r}) = \Psi_{\vec{k}+\vec{K}}(\vec{r}). \quad (1.12)$$

From the above equation we learn, that it is sufficient to know the wave function $\Psi_{\vec{k}}$ for wave vectors within the first Brillouin zone in order to describe the whole crystal.

From the properties of the reciprocal lattice vectors we can derive that any function $u(\vec{r})$ which is periodic within the lattice, can be represented by a Fourier series, which itself is periodic within the lattice.

$$u(\vec{r} + \vec{R}) = \sum_{\vec{K}} c(\vec{K})e^{i\vec{K}\vec{R}} \quad (1.13)$$

$$e^{i\vec{K}\vec{R}} = 1 \quad (1.14)$$

$$\vec{K}\vec{R} = 2\pi n \quad n \in N \quad (1.15)$$

This equation, however, is equivalent to equation 1.3, the definition of the reciprocal lattice vectors. Thus it follows that the vectors \vec{K} in the Fourier series must be the lattice vectors of the reciprocal lattice.

1.1.4 Born-Oppenheimer approximation

The system of interacting charged particles consist of nuclei and electrons. For this many-body problem we can write the exact many-particle Hamiltonian as follows:

$$\hat{H} = -\frac{\hbar^2}{2} \sum_a \frac{\nabla_{\vec{R}_a}^2}{M_a} - \frac{\hbar^2}{2} \sum_i \frac{\nabla_{\vec{r}_i}^2}{m_i} - \frac{1}{4\pi\epsilon_0} \sum_{a,j} \frac{e^2 Z_a}{|\vec{R}_a - \vec{r}_j|} \quad (1.16)$$

$$+ \frac{1}{8\pi\epsilon_0} \sum_{i \neq j} \frac{e^2}{|\vec{r}_i - \vec{r}_j|} + \frac{1}{8\pi\epsilon_0} \sum_{a \neq b} \frac{e^2 Z_a Z_b}{|\vec{R}_a - \vec{R}_b|} \quad (1.17)$$

with M_a being the mass and Z_a the charge of nucleus a at position \vec{R}_a , and m_e the electron mass at position \vec{r}_i .

These terms describe the kinetic energy operator for the nuclei (a, b) of the system, the kinetic energy operator of the electrons (i, j), the Coulomb interaction between electrons and nuclei, the Coulomb interaction between electrons with other electrons, and finally the last term is the Coulomb interaction between nuclei.

As nuclei are much heavier and thus much slower than electrons, we can assume them to be "frozen" at fixed positions, and the electrons will instantaneously equilibrate with them [2].

The consequence of this so called "Born-Oppenheimer approximation" on the Hamiltonian is as follows:

The nuclei do not move and therefore their kinetic energy is zero. The first term then disappears and the last term degenerates to a constant. Left are solely the terms for the kinetic energy of the electrons, the potential due to the electron-electron interaction and the potential energy of the electrons in an "external" potential caused by the "frozen" nuclei. This is formally written as:

$$\hat{H} = \hat{T} + \hat{V} + \hat{V}_{ext} \quad (1.18)$$

We note that in eq. 1.18 the first two terms, i.e. the kinetic energy and the electron-electron interaction term becomes independent of the nature of the interacting system. System specific information is carried entirely by \hat{V}_{ext} .

1.2 Density Functional Theory

1.2.1 Introduction

As already mentioned, the Schrödinger equation 1.1 cannot be solved exactly for many-electron systems. Therefore it is necessary to introduce approximations to solve it. There are two principal methods that are applied: the Hartree-Fock method (mainly used by theoretical chemists) and the Density Functional Theory (DFT). The latter was mainly used by theoretical physicists [40]. However DFT also has found its way into chemistry, which was officially appreciated by the Nobel committee by awarding the Nobel prize for chemistry to Walter Kohn in 1998 [1].

Already in the early sixties Hohenberg and Kohn worked on the problem of electrons in a periodic potential [15]. In this work they gave a proof that every observable of a stationary quantum mechanical system is determined by the ground state density alone.

The ground state energy of an interacting inhomogeneous electron system $E_{tot}[\rho(\vec{r})]$ in the presence of an external potential $V_{ext}(\vec{r})$ is a functional F of the charge density $\rho(\vec{r})$.

$$E_{tot}[\rho(\vec{r})] = \int V_{ext}(\vec{r})\rho(\vec{r})d\vec{r} + F[\rho(\vec{r})] \quad (1.19)$$

The exact ground state density of a system in a particular external potential $V_{ext}(\vec{r})$ is the density that minimizes $E_{tot}[\rho(\vec{r})]$.

For simplicity we will use in the following the case of a non spin-polarized system (equation 1.19), but generalization for spin polarized systems is possible and is realized in the code used.

As we can see, the charge density $\rho(\vec{r})$ is the basic variable in DFT. The functional $F[\rho(\vec{r})]$, which independent of the external potential $V_{ext}(\vec{r})$, is a universal density function, i.e. applicable to any arbitrary system.

Despite the formal proof of Hohenberg and Kohn's theorem the form of the functional F remains unknown. Therefore the functional is rewritten such that it is composed of the Hartree total energy plus a rest which is called the exchange-correlation functional, which must be approximated.

Thus we rewrite equation 1.19 in the following form:

$$E_{tot}(\rho) = T_s(\rho) + E_{ee}(\rho) + E_{Ne}(\rho) + E_{xc}(\rho) + E_{NN} \quad (1.20)$$

In this equation T_s is the kinetic energy of non-interacting particles, E_{ee} the electron-electron repulsion, E_{Ne} the nucleus-electron attraction, E_{NN} the repulsive Coulomb interaction between the nuclei, and E_{xc} the exchange-correlation energy.

According to this definition, the exchange-correlation energy E_{xc} is given by the difference between the real total energy and the sum of the known terms. Thus the unknown functional from equation 1.19 has been reduced to the (still unknown) functional for the exchange-correlation energy. This, however can be approximated e.g. by the "Local Density Approximation" (LDA) or the "Generalized Gradient Approximation" (GGA).

1.2.2 Local Density Approximation

In the Local Density Approximation (LDA) the exchange-correlation energy is approximated by E_{xc}^{LDA} (equation 1.21), where ε_{xc}^{LDA} is the exchange-correlation density of a homogeneous electron gas, which only depends on the electron density $\rho(\vec{r})$, thus the name "local density approximation".

$$E_{xc}^{LDA}[\rho(\vec{r})] = \int \rho(\vec{r}) \varepsilon_{xc}[\rho(\vec{r})] d\vec{r} \quad (1.21)$$

This exchange correlation energy can be split into two components:

$$E_{xc}^{LDA} = E_x^{LDA} + E_c^{LDA} \quad (1.22)$$

The first contribution E_x^{LDA} is the exchange energy that comes from the Pauli exclusion principle. In the local density approximation it is assumed that at any position \vec{r} the exchange energy of the real system (inhomogeneous electron gas) can be substituted by the corresponding energy of the homogeneous electron gas of the same density. For the latter the exact formulation is known and scales approximately as:

$$E_x \propto \rho^{\frac{4}{3}} \quad (1.23)$$

The second contribution, called the correlation energy E_c^{LDA} , originates from the interaction of electrons having the same spin. Both terms E_x and E_c can be calculated using quantum Monte-Carlo methods [7]. In our code the parametrization from Perdew and Wang [42] is implemented.

1.2.3 Generalized Gradient Approximation

Whereas LDA uses the exchange energy density of the uniform electron gas, regardless of the inhomogeneity of the real charge density, the generalized gradient approximation takes care of such inhomogeneities by including the gradient of the electron density in the functional.

$$E_{xc}^{GGA}[\rho(\vec{r})] = \int \varepsilon_{xc}[\rho(\vec{r}), \nabla\rho(\vec{r})]\rho(\vec{r})d\vec{r} \quad (1.24)$$

For practical calculations a parametrized form of the functional ε_{xc}^{GGA} must be implemented. The parametrization used for the calculations in this work are those of Perdew, Burke and Ernzerhof [41].

1.2.4 The Kohn-Sham equations

Starting with eq. 1.20 we derive the following one-electron equations by forming the derivate of the total energy with respect to the electron density, such that the change in electron density is zero. This leads to the so called Kohn-Sham equations [23]:

$$\{-\nabla^2 + V_c(\vec{r}) + V_{xc}[\rho(\vec{r})]\} \Phi_i(\vec{r}) = \varepsilon_i \Phi_i(\vec{r}) \quad (1.25)$$

$$\rho(\vec{r}) = \sum_{i_{occupied}} |\Phi_i|^2 \quad (1.26)$$

where V_{xc} is the exchange correlation potential, which is defined by

$$V_{xc}[\rho(\vec{r})] = \frac{\partial E_{xc}[\rho(\vec{r})]}{\partial \rho(\vec{r})} \quad (1.27)$$

From equation 1.27 we readily see that the exchange correlation potential is only dependent on the electron density ρ at position \vec{r} and thus is a local potential.

Equation 1.25 is structurally identical to the Schrödinger equation (1.1). As the multi-electron equations have been reduced to a single-electron Schrödinger equation, the problem can now be solved.

1.3 The Variational Principle

The Rayleigh-Ritz variational principle provides a powerful mechanism for finding ground state energies. It is based on the fact, that the expectation value of any trial function is always greater than the eigenvalue of the exact wavefunction.

Since the exact wavefunction is not known, we construct a trial function Ψ_k as a linear combination of basis functions ϕ_i which are weighted by coefficients C_i :

$$\Psi_k = \sum_{i=1}^n C_i \phi_i \quad (1.28)$$

The expectation value for the energy $\langle E \rangle$ can then be written as

$$\langle E \rangle = \frac{\int \Psi_k^*(C_1, \dots, C_n) \hat{H} \Psi_k(C_1, \dots, C_n) d\mathbf{r}}{\int \Psi_k^*(C_1, \dots, C_n) \Psi_k(C_1, \dots, C_n) d\mathbf{r}}. \quad (1.29)$$

Minimization of $\langle E \rangle$ requires that the derivatives with respect to C_i (for $i = 1, \dots, n$) must vanish, which yields a set of secular equations:

$$\sum_{j=1}^n (H_{ij} - \epsilon_i S_{ij}) C_j = 0 \quad (1.30)$$

$$H_{ij} = \int \phi_i^* \hat{H} \phi_j d^3\mathbf{r} \quad (1.31)$$

$$S_{ij} = \int \phi_i^* \phi_j d^3\mathbf{r} \quad (1.32)$$

where H_{ij} are matrix elements of the single-particle Kohn-Sham Hamiltonian \hat{H} , and S_{ij} the elements of the overlap matrix. This represents a general eigenvalue problem. Once we know ϵ_i we can substitute it in equation 1.30, determine the coefficients C_j and thus define the trial function Ψ_k . The obtained eigenvalues are real, since the Hamiltonian and the overlap matrix are hermitian.

If the basis functions are independent of energy, the problem reduces to a general eigenvalue problem, and the eigenvalues ϵ_i are obtained by diagonalization according to equation 1.30.

1.4 The "Self Consistent Field (SCF)"

In the previous section we have described how to reduce the complex problem of many interacting particles to a Schrödinger-like equation. In order to solve these equations, we have to construct the effective Hamilton operator.

The problem, however, is that parts of this Hamilton operator depend on the electron density, which can only be derived from the solution of the Kohn-Sham equations. To

solve this problem, we use the iterative method called "*Self Consistent Field*" (SCF) as follows:

Initially we use atomic densities at the positions of the atoms in the crystal. From such a crystalline density we can set up the Hamilton operator. From this we derive an electron density in the crystal by solving the Kohn-Sham equations and summing the electron density of all occupied states. From this new electron density we can calculate a new potential and from this again a new Hamilton operator.

We repeat these steps as often as necessary to satisfy predefined convergence criteria (e.g. constant total energy). The converged results are then independent of the starting potential, and therefore self consistent.

A prerequisite for a good convergence and a small number of iterations is a good starting potential and an efficient procedure to mix old (input) and new (output) electron densities after each iteration.

1.5 The Linearized Augmented Plane Wave Method

1.5.1 Introduction

To solve the Kohn-Sham equations 1.25 [23] a number of different methods have been developed. From the Bloch Theorem (see section 1.1.3) boundary conditions for the single particle wave function can be derived. A general solution for these wave functions can be obtained with *plane waves*. Madelung [30] has shown that plane waves constitute a complete and orthogonal basis set. However, strong fluctuations appear in the wave function close to the nucleus. To describe these features a huge number of plane waves would be required. To reduce the number of plane waves, Slater suggested in 1937 to augment the plane wave basis set in the region of the atomic spheres with basis functions that are more appropriate for the description of atomic wave functions. This resulted in the Augmented Plane Wave method [57]. However, this particular basis set leads to a non-linear eigenvalue problem, which is hard to solve. In 1975 Andersen suggested to expand the energy dependence of radial wave functions inside the atomic spheres with its energy derivative and thus established the Linearized Augmented Plane Wave (LAPW) method [3].

1.5.2 Basis Set in the LAPW method

In the LAPW method the unit cell is divided into non overlapping regions (see figure 1.1): the region of the atomic spheres (I), and the region of the remaining volume, the so called "interstitial" (II).

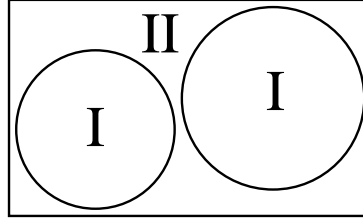


Figure 1.1: Division of the unit cell in the LAPW method

The radius of the non-overlapping atomic region is called "muffin-tin" radius. It is usually chosen as big as possible, but always under the condition, that the spheres do not overlap.

Within the interstitial region the wave function is expanded in by plane waves having Bloch-form:

$$\phi_{\vec{k}_n} = \frac{1}{\sqrt{\Omega}} e^{i\vec{k}_n \vec{r}} \quad (1.33)$$

$$(1.34)$$

with $\vec{k}_n = \vec{k} + \vec{K}_n$ and \vec{k} being the wave vector of the first Brillouin zone and \vec{K}_n a reciprocal lattice vector.

To avoid the huge number of plane waves to describe the wave function near the nucleus, the basis set is augmented: Within an atomic sphere t the wave function is represented by a linear combinations of radial functions $u_l(r, E_l)$ multiplied with the angular dependent lattice harmonics $Y_{lm}(\hat{r})$.

The radial parts can be calculated from a numerical outward integration of the radial Schrödinger equation along a radial mesh:

$$\left\{ -\frac{d^2}{dr^2} + \frac{l(l+1)}{r^2} + V(r) - E \right\} ru(r, E) = 0 \quad (1.35)$$

From equation 1.35 we see that the radial functions are functions of the energy, which would lead to energy dependent secular equations which can be solved by the repeated calculation of the secular determinant. This was done in the original APW method [57].

In the LAPW method we linearize the radial functions and thus the problem is reduced to a linear eigenvalue problem. We do this by a Taylor expansion of the radial function to first order.

$$u_l(r, E) \simeq u(r, E_l) + \dot{u}(r, E_l) \quad (1.36)$$

The linearization energy E_l is chosen such, that it is close to the expected eigenvalue. Therefore we can write the wave function within the atomic sphere as:

$$\phi_{k_n} = \sum_{lm} [A_{lm}u_l(r, E_l) + B_{lm}\dot{u}_l(r, E_l)]Y_{lm}(\hat{r}) \quad (1.37)$$

The coefficients A_{lm} and B_{lm} are functions of k_n and are calculated under the conditions that the wave function must be continuous in value and slope at the sphere boundary.

1.5.3 Solving the Schrödinger equation

Using the above basis set, we can now solve the one-electron Kohn-Sham equations (equation 1.25) using the Rayleigh-Ritz variational principle (see section 1.3).

The elements of the Hamilton- and the overlap-matrix are calculated, and the resulting generalized eigenvalue problem (equation 1.35) is solved. For the calculation of the Hamilton matrix elements a "full potential" is used, i.e. there is no approximation in the description of the potential. The potential is represented by a Fourier series in the interstitial and by radial dependent times lattice harmonics functions inside the atomic spheres [5, 6].

The results of the generalized eigenvalue problem are energy eigenvalues of the crystal wave function from which the variational coefficients of the trial function (see section 1.3) can be calculated.

The crystal wave function can be solved for different k-points of the first Brillouin zone. To increase the accuracy of the calculation, a finer k-mesh has to be chosen. Showing the energy eigenvalues along certain symmertry lines of the Brillouin zone results in a so called bandstructure plot. The weighted number of states vs. energy yields the density of states (DOS).

$$g(\varepsilon) = V_{BZ} \int_{BZ} \delta(\varepsilon - \varepsilon_{\vec{k}_i, b}) d\vec{k}_i \quad (1.38)$$

where V_{BZ} is the volume of the first Brillouin zone.

1.5.4 The electron density

Occupying the energy levels according to the aufbau principle (with weight w_i) with electrons until all electrons are used results in the Fermi level. The Fermi level is the

highest occupied energy level. The electron density $\rho(\vec{r})$ is given by a summation over all occupied levels $\varepsilon(\vec{k}_i, \nu)$ (see also equation 1.26), where ν is the band index and w_i is the weight of the star of the k-vectors.

$$\rho(\vec{r}) = \sum_{i,\nu} w_i \rho_{\vec{k}_i,\nu}(\vec{r}) \quad (1.39)$$

$$\varepsilon(\vec{k}_i, \nu) \leq E_F \quad (1.40)$$

$$\rho_{\vec{k}_i,\nu}(\vec{r}) = \Psi \rightarrow *_{\vec{k}_i,\nu}(\vec{r}) \Psi_{\vec{k}_i,\nu}(\vec{r}) \quad (1.41)$$

The electron density is represented by lattice harmonics within atomic spheres and by a Fourier series in the interstitial region

$$\rho(\vec{r}) = \begin{cases} \sum_{LM} \rho_{LM}(r) f_{LM} Y_{LM}(\hat{r}) & \text{atomic sphere} \\ \sum_n \rho(\vec{K}_n) e^{i\vec{K}_n \vec{r}} & \text{interstitial} \end{cases} \quad (1.42)$$

where f_{LM} is a constant given by symmetry.

Lattice harmonics are linear combinations of spherical harmonics having the point group symmetry of the corresponding atom [25]. This means, that within the atomic spheres, a local coordinate system has to be chosen, which obeys this condition. This also ensures, that an efficient basis set (i.e. as small as possible) is chosen.

1.5.5 The potential and total energy

The potential $V(\vec{r})$ is given by two components:

$$V(\vec{r}) = V_{coul}(\vec{r}) + V_{xc}(\vec{r}) \quad (1.43)$$

the Coulomb potential $V_{coul}(\vec{r})$, and $V_{xc}(\vec{r})$ the exchange-correlation potential, which is due to the Pauli exclusion principle.

The Coulomb potential can easily be derived from the total electron density by solving the Poisson equation[54]:

$$\nabla^2 V_{coul}(\vec{r}) = -8\pi\rho(\vec{r}) \quad (1.44)$$

The second part, the exchange-correlation potential, is also calculated from the total electron density using the local density approximation (see section 1.2.2) or the generalized gradient approximation (see section 1.2.3).

The total potential (like the electron density) is represented by lattice harmonics and a Fourier series.

$$V(r) = \begin{cases} \sum_{LM} V_{LM}(r) Y_{LM}(\hat{r}) & \text{atomic sphere} \\ \sum_K V_K e^{iKr} & \text{interstitial} \end{cases} \quad (1.45)$$

Thus the total energy of the system per unit cell can be calculated from the electron density according to Hohenberg and Kohn (eq. 1.19). It consists of the following contributions: the kinetic, the potential and the exchange-correlation energies (see equation 1.20).

The absolute value of the calculated total energies has no so much physical relevance because LDA and GGA are only rough estimates. However, differences in the total energy can be calculated accurately and are relevant for relative stabilities.

1.5.6 Description of electronic states

In a solid one can distinguish electronic states that have different properties. They are called core, semicore and valence states.

Core states

These are electronic states having a very low energy (normally less than approx. -7 Ryd). These states are strongly localized around the nucleus and their corresponding charge density is completely confined inside the atomic sphere. As these states do not interact with other electronic states, they can be treated separately. They can be calculated by solving the relativistic atomic Dirac equation in the potential of the crystal. At the sphere boundary (muffin-tin radius) the wave functions of these states should be zero in order to obey orthogonality.

The calculation results in a spherically symmetric charge distribution of these state

$$\rho_{core} = \rho(r) Y_{0,0}(\hat{r}) \quad (1.46)$$

where r is the distance from the nucleus.

Semi-core states

These states lie in an energy range between approximately -7 and -2 Ryd and the corresponding charge density leaks outside the sphere. Their interaction with valence states is not negligible. However, their interaction, and thus their influence on the k -dispersion (i.e. the dependence of the energy eigenvalues on the wave vector \vec{k} ; see section 1.1.3) is small.

Semi-core states can be included in the calculation of valence states by introducing so called “local orbitals” [52, 53]:

$$\phi_{k_n}^{LO} = \sum_{lm} [A_{lm}u_l(r, E_{1,l}) + B_{lm}\dot{u}_l(r, E_{1,l}) + C_{lm}u_l(r, E_{2,lm})]Y_{lm}(\hat{r}) \quad (1.47)$$

Thus local orbitals are constructed from two radial functions at different energies (corresponding to principle quantum numbers n and $n+1$) plus one energy derivative at one of the energies. The coefficients A_{lm} , B_{lm} and C_{lm} are chosen such to make the LO vanish in both, value and slope, at the sphere boundary. The advantages of using local orbitals are:

- no separate calculation of semi-core states is necessary,
- local orbitals ensure that semi-core states are orthogonal to valence states, and
- local orbitals can be used to describe unoccupied states at higher energies, which can be important for the calculation of spectra [43]).

Valence States

Valence states are responsible for chemical bonding. They have a high k-dispersion, thus a large number of k-points is necessary for their proper description.

1.5.7 Summation of states

To describe all states of a crystal, all different states described above, have to be summarized. Within DFT the easiest way to accomplish this is via electron densities, which were formally written in the same form. Simply adding the coefficients will yield the total electron density (equation 1.39) from which the potential is calculated.

1.6 The APW+lo method

Sjöstedt, Nordström and Singh [55, 56] have demonstrated that the standard LAPW method is not the most efficient way to linearize Slater’s APW method. Efficiency can be increased by lifting the constraint that each plane wave must match in value **and** slope to the solutions inside the atomic spheres.

By using the standard APW basis, however, with $u_l(r, E_l)$ at a fixed energy E_l (in order to keep the linear eigenvalue problem) one can increase the efficiency.

To have enough variational flexibility in the radial basis functions a new local orbital (lo) is added:

$$\phi_{\mathbf{k}_n} = \sum_{lm} [A_{lm, \mathbf{k}_n} u_l(r, E_l)] Y_{lm}(\hat{\mathbf{r}}) \quad (1.48)$$

$$\phi_{lm}^{lo} = [A_{lm} u_l(r, E_{1,l}) + B_{lm} \dot{u}_l(r, E_{1,l})] Y_{lm}(\hat{\mathbf{r}}) \quad (1.49)$$

This new local orbital lo (in lower case to distinguish it from the conventional local orbitals LO in eq. 1.47) looks much like the LAPW basis set, but here the A_{lm} and B_{lm} are not dependent on k_n . They are determined by the requirement that the lo is normalized and its value is zero at the sphere boundary.

The new type of basis functions have "kinks" at the sphere boundary. This makes it necessary to include surface terms in the kinetic energy part of the Hamiltonian. The total wavefunction, however, is smooth and differentiable.

Madsen et al. [31] have shown that this scheme converges to practically identical results as the conventional LAPW method, but allows to reduce the parameter $R_{mt} * k_{max}$ by about one, thus leading to significantly smaller basis set and therefore reducing the computation time dramatically (up to an order of magnitude).

1.7 Simulation of core-level spectra

1.7.1 Introduction

In core level spectroscopies we are interested in the absorption (or emission) fine structure in the range of 20–40 eV above (or below) the edge. Due to the fact that core states are involved in this type of spectroscopy, site specific information is obtained.

Whereas in Electron Energy Loss Spectroscopy (EELS) we use electrons to excite core states into unoccupied conduction band levels, in X-ray experiments X-photons are utilized. However, the theoretical descriptions of both X-ray and EELS experiments are very similar [18]. Both derivations start from Fermi's Golden rule within first order perturbation theory. More details are given below.

The considerations for the calculation of absorption spectra can be directly used for emission spectra as well, if provision is taken that initial and final states are interchanged.

Rez [45] has given a marvellous review of the various methods for the calculation of spectra with a near edge structure. A hierarchy of approximations for the calculation of near edge structures can be given:

1. Atomic Wave Function
the basic edge shape can be calculated but no fine structure; the maxima are shifted
2. Single Scattering Approach
the atomic wave functions are reflected from neighboring atoms. This approach works well for the so called "extended structure" (approx. 50 eV to several hundreds eV above the edge).
3. Full Multiple Scattering Approach
Multiple scattering allows for multiple reflection of the wave functions. The potential is constructed by the superposition of ion cores. The calculation is carried out in a non-self-consistent manner and does not give a good representation of the states near the threshold.
4. Self-Consistent one-electron band theory methods.
Unoccupied states are calculated in a self-consistent potential. The methods for the self-consistent calculation of the potential are manifold, e.g. APW (augmented plane waves), ASW (augmented spherical waves), KKR (Korringa-Kohn-Rostoker), or LAPW (linearized augmented plane waves).
These methods directly yield the local angular momentum resolved densities of states.
5. Inclusion of Core-hole effects.

In this work a self-consistent one-electron band theory method, namely (L)APW+lo has been used. Furthermore the effects of the core-hole have been investigated using the same method but applied to numerous materials. Other methods will not be covered by this work.

1.7.2 Inelastic scattering of electrons in a solid

The definition of elastic and inelastic scattering depends on the target [46]. In the case of elastic scattering the inner energy of the system (i.e. target and incident particle) does not change. If, however, the inner energy changes, the scattering process is called inelastic.

Scattering between two electrons is always elastic, as the sum of the kinetic energies of both electrons remains unchanged before and after the scattering process.

In a solid the scattering process is always inelastic as the inner energy of the target changes due to the excitation of electrons from occupied to higher, unoccupied energy levels [13]. A typical case of an inelastic process is the interaction of a fast incident electron with an atom, exciting a core electron to a higher energy level (see figs. 1.2 and 1.3).

In a Transmission Electron Microscope (TEM) the interaction of a fast electron (200 keV) with the target sample are described by such inelastic scattering processes.

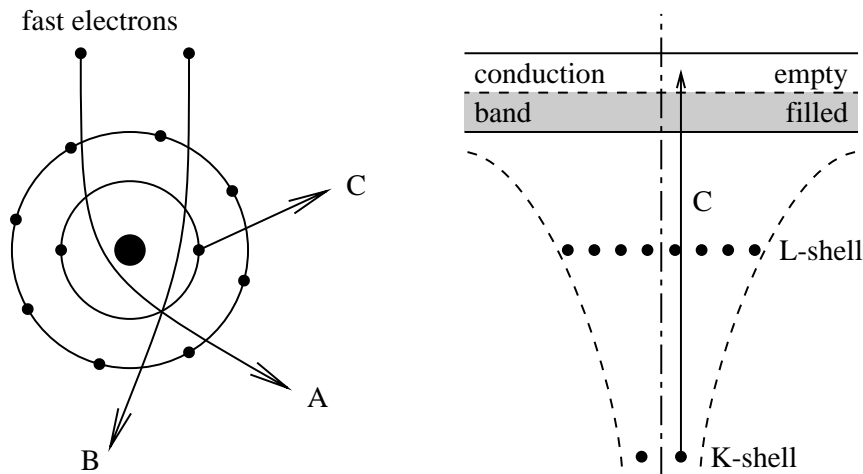


Figure 1.2: electron scattering [9]

By use of a Parallel Electron Energy Loss Spectrometer (PEELS) it is possible to count the transmitted electrons according to their energy. This yields the electron energy loss spectrum (EELS), i.e. the number of detected electrons as a function of their energy loss (see fig. 1.4).

1.7.3 Energy Loss Near Edge Structure

The Energy Loss Near Edge Structure (ELNES) describes the structure of the edge up to approx. 30 eV above the edge onset (see fig. 1.4). In this region, which can be measured with only a few percent of experimental error, the spectrum describes in principle the density of unoccupied electron states of the crystal.

For an incident electron to lose a certain amount of energy by an inelastic scattering process, it must excite a core electron of the target atom with exactly this amount of energy. The core electron is in due course excited to an unoccupied state above the Fermi level. The probability for this process is proportional to the number of empty states, which are given by the density of states DOS (see eq. 1.38).

The local density of (unoccupied) states depends on the crystal structure, the atoms, the atom positions and also on the chemical environment of the target.

1.7.4 The Dynamic Form Factor

The probability per unit time for a certain transition between an initial state $|i\rangle$ and a final state $|f\rangle$ can be given by Fermi's Golden Rule (see [14]):

$$dW_{if} = 2\frac{\pi}{\hbar} \left| \langle f|V|i\rangle \right|^2 dv_f \delta(E_i - E_f) \quad (1.50)$$

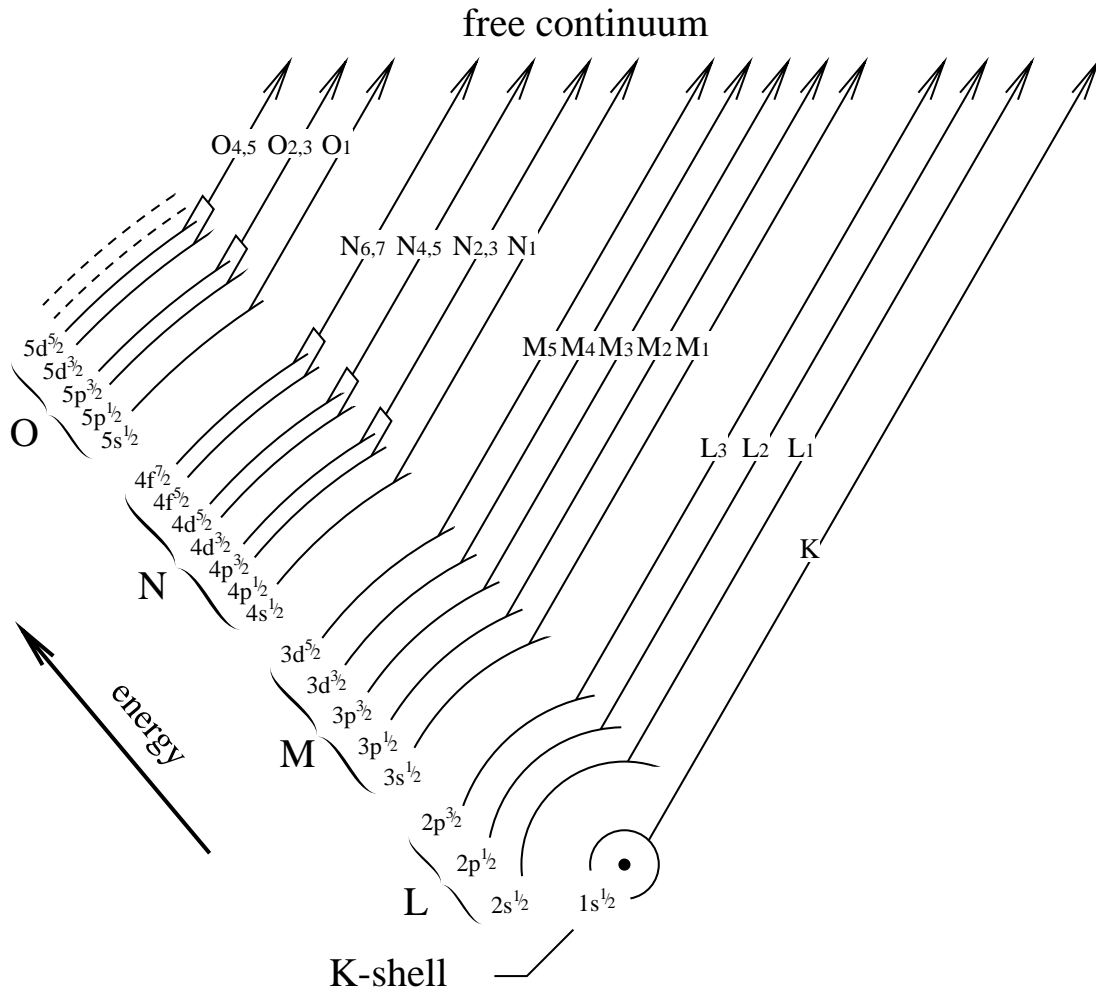


Figure 1.3: Electron transitions

In equation 1.50 E_i and E_f denote the initial and final energies of the system, dv_f the differential volume element in phase space, and V the Coulomb potential between the two electrons.

The initial and final states are given by

$$|i\rangle = |\mathbf{k}_i\rangle \otimes |nlm\rangle, \quad |f\rangle = |\mathbf{k}_f\rangle \otimes |\mathbf{k}\nu\rangle \tag{1.51}$$

where $|\mathbf{k}_i\rangle$ and $|\mathbf{k}_f\rangle$ represent the initial and final states of the incident electron, $|nlm\rangle$ the initial state of the core electron (represented by the quantum numbers n , ℓ and m) and $|\mathbf{k}\nu\rangle$ its final state (valence state, characterized by the band index ν and the \mathbf{k} -vektor in the Brillouin zone).

We can write the differential electron current as

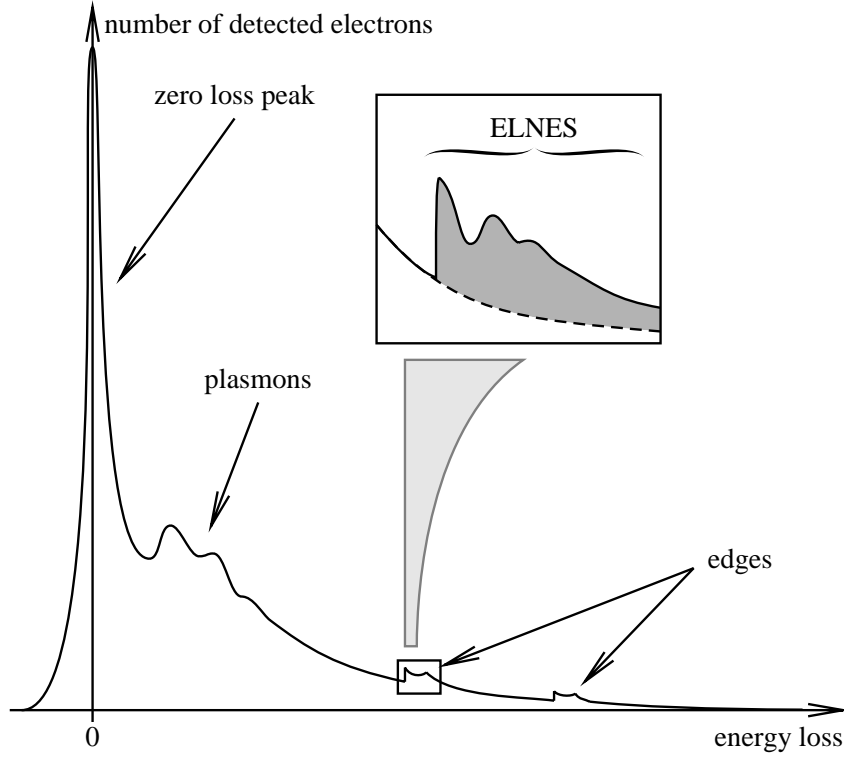


Figure 1.4: typical energy loss spectrum

$$dj(dE, d\Omega) = \frac{\partial W}{\partial \Omega \partial E} d\Omega dE \quad (1.52)$$

or as

$$d\sigma = \sum_{if} \frac{(2\pi)^3 m_e}{\hbar k_i} dW_{if} \quad (1.53)$$

with

$$dW_{if} = \frac{2\pi}{\hbar} \langle \mathbf{k}\nu | \otimes \langle \mathbf{k}_f | V | \mathbf{k}_i \rangle \otimes | n\ell m \rangle dv_f \delta(E + E_{n\ell m} - E_{\kappa\nu}). \quad (1.54)$$

Using the relation $dv_f = \frac{2m_e}{\hbar} k_f dE d\Omega$ yields

$$\frac{\partial^2 \sigma}{\partial \Omega \partial E} = \left(\frac{2\pi}{\hbar} \right)^4 m_e^2 \frac{k_f}{k_i} \sum_{\substack{\mathbf{k}, \nu \\ n, \ell, m}} \left| \langle \mathbf{k}\nu | \otimes \langle \mathbf{k}_f | V | \mathbf{k}_i \rangle \otimes | n\ell m \rangle \right|^2 \delta(E + E_{n\ell m} - E_{\kappa\nu}). \quad (1.55)$$

Equation 1.55 gives the number of scattered electrons per energy unit as a function of their energy loss E .

To calculate the ELNES of an edge, we need a solution of this equation in the energy range of E_{edge} to $E_{\text{edge}} + 30$ eV. Equation 1.55 would require an integration in 6-dimensional space (over \mathbf{r} of the fast electron and \mathbf{R} of the core electron). To avoid this the formula is converted analytically.

Thus it is possible to simplify the matrix element $\langle \mathbf{k}_f | V | \mathbf{k}_i \rangle$: in the case where the fast electron can be described as a plane wave, this matrix element is exactly the Fourier transform of the Coulomb potential between the fast electron and the core electron ($n\ell m$ at position \mathbf{R}):

$$\langle \mathbf{r} | \mathbf{k}_i \rangle = (2\pi)^{-\frac{3}{2}} e^{i\mathbf{k}_i \cdot \mathbf{r}} \quad \text{and} \quad \langle \mathbf{r} | \mathbf{k}_f \rangle = (2\pi)^{-\frac{3}{2}} e^{i\mathbf{k}_f \cdot \mathbf{r}} \quad (1.56)$$

$$\begin{aligned} \langle \mathbf{k}_f | V | \mathbf{k}_i \rangle &= \frac{1}{(2\pi)^3} \int d^3r \frac{e_0^2}{|\mathbf{r} - \mathbf{R}|} e^{i(\mathbf{k}_i - \mathbf{k}_f) \cdot \mathbf{r}} \\ &= \frac{e_0^2}{2\pi^2 q^2} e^{i\mathbf{q} \cdot \mathbf{R}} \quad \text{with } \mathbf{q} = \mathbf{k}_i - \mathbf{k}_f \end{aligned} \quad (1.57)$$

This yields a simple expression for the differential cross section of equation 1.55:

$$\frac{\partial^2 \sigma}{\partial \Omega \partial E} = 4 \left(\frac{e_0}{q} \right)^4 m_e^2 \frac{k_f}{k_i} \sum_{\substack{\mathbf{k}, \nu \\ n, \ell, m}} \left| \langle \mathbf{k} \nu | e^{i\mathbf{q} \cdot \mathbf{R}} | n\ell m \rangle \right|^2 \delta(E + E_{n\ell m} - E_{\kappa\nu}) \quad (1.58)$$

The sum is now defined as the dynamic form factor

$$S(\mathbf{q}, E) = \sum_{\substack{\mathbf{k}, \nu \\ n, \ell, m}} \left| \langle \mathbf{k} \nu | e^{i\mathbf{q} \cdot \mathbf{R}} | n\ell m \rangle \right|^2 \delta(E + E_{n\ell m} - E_{\kappa\nu}). \quad (1.59)$$

1.7.5 Near Edge electron energy loss spectra (ELNES)

For near edge Electron Energy Loss Spectra Schattschneider and Nelhiebel [49, 37] define the double differential scattering cross section for the excitation of an atom by a fast electron as

$$\frac{\partial^2 \sigma}{\partial E \partial \Omega} = \frac{4\gamma^2}{a_0^2} \frac{k}{k_0} \frac{1}{Q^4} S(\mathbf{Q}, E). \quad (1.60)$$

They define the Dynamic Form Factor (DFF) as

$$S(\mathbf{Q}, E) = \sum_{i,f} |\langle i | e^{-i\mathbf{Q}\mathbf{R}} | f \rangle|^2 \delta(E + E_i - E_f) \quad (1.61)$$

where a_0 is the Bohr radius, $\gamma = \sqrt{1 - \beta^2}$ the relativistic factor, and k_0, k the length of the fast electron's wave vectors \mathbf{k}_0 and \mathbf{k} before and after interaction. The scattering vector is defined as $\mathbf{Q} = \mathbf{k}_0 - \mathbf{k}$. In those cases where the dipole approximation is justified, we can write $e^{i\mathbf{Q}\mathbf{R}} \simeq 1 + i\mathbf{Q}\mathbf{R}$. Then the direction of \mathbf{Q} plays the same role as the polarization vector $\vec{e}\vec{P}$ in X-ray absorption spectra. Thus the formulae derived for Electron Energy Loss Spectrometry may also be applied to XAS [26] as long as the dipole approximation remains valid.

However, in contrast to XAS where the momentum transfer is always zero, the scattering vector \mathbf{Q} is sensibly dependent on the direction between the incident and outgoing wave vectors. Therefore even for small momentum transfers the dipole approximation can become insufficient when looking at angular resolved spectra in EELS.

Nelhiebel et al. [37] have given three formulae for the calculation of the DFF within the framework of WIEN2k. The simplest formula they present is for averaging over all directions (e.g. when looking at polycrystalline samples) and thus is equivalent to equation 1.78 for the calculation of X-ray spectra:

$$S(\mathbf{Q}, \mathbf{Q}', E) = o_{j\ell} \sum_{\ell'=0}^{\ell'_{\max}} \sum_{\lambda=|\ell-\ell'|}^{\ell+\ell'} \rho_{\ell'}(E_{n_{j\ell}} + E) P_{\lambda}(\cos \alpha) [\lambda] \begin{pmatrix} \ell & \lambda & \ell' \\ 0 & 0 & 0 \end{pmatrix}^2 \langle j_{\lambda}(Q) \rangle_{n\nu\mathbf{k}\ell\ell'} \langle j_{\lambda}(Q') \rangle_{n\nu\mathbf{k}\ell\ell'} \quad (1.62)$$

The other two formulae include orientation dependence of the sample relative to the incident electron beam. For crystals with at least orthorhombic symmetry the equation reads:

$$S(\mathbf{Q}, \mathbf{Q}', E) = 4\pi o_{j\ell} \sum_{\ell'=0}^{\ell'_{\max}} \sum_{\lambda=|\ell-\ell'|}^{\ell+\ell'} [\ell'] [\lambda]^{\frac{1}{2}} \langle j_{\lambda}(Q) \rangle_{n\nu\mathbf{k}\ell\ell'} \begin{pmatrix} \ell & \lambda & \ell' \\ 0 & 0 & 0 \end{pmatrix} \sum_{\lambda'=|\ell-\ell'|}^{\ell+\ell'} i^{\lambda-\lambda'} [\lambda']^{\frac{1}{2}} \langle j_{\lambda'}(Q') \rangle_{n\nu\mathbf{k}\ell\ell'} \begin{pmatrix} \ell & \lambda' & \ell' \\ 0 & 0 & 0 \end{pmatrix} \sum_{\mu=-\lambda}^{+\lambda} \sum_{\mu'=-\lambda'}^{+\lambda'} Y_{\mu}^{\lambda}(\tilde{\mathbf{Q}})^* Y_{\mu'}^{\lambda'}(\tilde{\mathbf{Q}}') \sum_{m=-\ell}^{+\ell} \sum_{m'=-\ell'}^{+\ell'} \rho_{\ell'm'}(E_{n_{j\ell}} + E) \begin{pmatrix} \ell & \lambda & \ell' \\ -m & \mu & m' \end{pmatrix} \begin{pmatrix} \ell & \lambda' & \ell' \\ -m & \mu' & m' \end{pmatrix}. \quad (1.63)$$

To calculate angular resolved spectra of highly anisotropic crystals with symmetries lower than orthorhombic the following formula must be used:

$$\begin{aligned}
S(\mathbf{Q}, \mathbf{Q}', E) = & 4\pi \rho_{j\ell} \sum_{\ell'=0}^{\ell'_{\max}} \sum_{\lambda=|\ell-\ell'|}^{\ell+\ell'} [\ell'] [\lambda]^{\frac{1}{2}} \langle j_{\lambda}(Q) \rangle_{n\nu\mathbf{k}\ell\ell'} \begin{pmatrix} \ell & \lambda & \ell' \\ 0 & 0 & 0 \end{pmatrix} \\
& \sum_{\lambda'=|\ell-\ell'|}^{\ell+\ell'} i^{\lambda-\lambda'} [\lambda']^{\frac{1}{2}} \langle j_{\lambda'}(Q') \rangle_{n\nu\mathbf{k}\ell\ell'} \begin{pmatrix} \ell & \lambda' & \ell' \\ 0 & 0 & 0 \end{pmatrix} \\
& + \min(\lambda, \lambda') \\
& \sum_{\mu=-\min(\lambda, \lambda')} Y_{\mu}^{\lambda}(\tilde{\mathbf{Q}})^* Y_{\mu}^{\lambda'}(\tilde{\mathbf{Q}}') \\
& \sum_{m=-\ell}^{+\ell} \rho_{\ell' m-\mu} (E_{nj\ell} + E) \begin{pmatrix} \ell & \lambda & \ell' \\ -m & \mu & (m-\mu) \end{pmatrix} \begin{pmatrix} \ell & \lambda' & \ell' \\ -m & \mu & (m-\mu) \end{pmatrix}.
\end{aligned} \tag{1.64}$$

All of these formulae have been implemented into WIEN2k as the module `e1nes` (see 2.3).

1.7.6 TELNES.2 - new development

New developments in the theory of ELNES in anisotropic materials have shown that a fully relativistic treatment of the incident electron is necessary to obtain correct cross sections because relativity acts in opposite ways on the components of the momentum transfer parallel and perpendicular to the incoming electrons velocity [47, 17].

In this section we present Bethe's fully relativistic theory as developed in [47] but extended beyond the dipole approximation [22].

General formalism

The central quantity in our theory is the double differential scattering cross section (DDSCS), which gives the probability of exciting the sample from an initial to a final state by absorbing a certain energy and impuls from the electron beam. These initial and final states are taken to be one electron states (i.e., we pretend that the electron beam interacts with one electron of the sample and leaves the rest of the sample unchanged). The aim of this chapter is to derive an expression for the double differential scattering cross section that will be of use for the calculation and interpretation of ELNES. The result has to be fully relativistic, has to capture the sensitivity of an EELS experiment to the sample to beam orientation, and has to allow for interpretation of the cross section in terms of the orbital momentum l -character of the final state.

We make three additional assumptions :

- Diffraction effects are not important (i.e., either there is no diffraction, or we are working in one diffraction spot (eg. the 000 spot) and the others may be ignored. This implies that the cross section is fully determined by the dynamic form factor (DFF). Cross terms in the impuls transfer vector \mathbf{q} , which require the use of the mixed dynamic form factor (MDFF) [38], do not occur.
- The initial state is a sharp state with zero energy width. This limits the applicability of our results to transitions from core states to unoccupied states and excludes very low energy edges and valence to unoccupied state transitions.
- We are working in a crystal and therefore the final state is a Bloch state.

A relativistic expression for the DDSCS has recently been presented in [47]. We use equation 12 of [47] (repeated as eq. 1.65 below) as starting point . We then elaborate the equations in a similar way as in [38]. We expand all quantities in spherical harmonics and solve the integrals over the angular coordinates using properties of the spherical harmonics. We also introduce spin quantum numbers in the equation, as in [48].

The DDSCS for scattering with energy loss E in a direction specified by the solid angle Ω (related to \mathbf{q} in the right hand side of the equation), is given by

$$\begin{aligned} \frac{\partial^2 \sigma}{\partial E \partial \Omega} &= \frac{4a_0^{-2}}{q^2 - (E/\hbar c)^2} \frac{k'}{k} \sum_{i,f} |\langle i | e^{i\mathbf{q}\cdot\mathbf{r}} (1 - \frac{\mathbf{p}\cdot\mathbf{v}_0}{m_e c^2}) | f \rangle|^2 \delta(E_f - E_i - E) \\ &= \frac{4a_0^{-2}}{q^2 - (E/\hbar c)^2} \frac{k'}{k} \text{DFF}(\mathbf{q}, E) \end{aligned} \quad (1.65)$$

where i are initial states of energy E_i , f are final states of energy E_f , the impuls transfer vector or scattering vector $\mathbf{q} = \mathbf{k} - \mathbf{k}'$, where \mathbf{k} is the wave vector of the incident fast electron and \mathbf{k}' the wave vector of the scattered electron and \mathbf{v}_0 is the velocity of the incident electron, a_0 is the Bohr radius, and m_e the electron rest mass.

We use the principal quantum number n , the orbital number l_i and the relativistic quantum numbers j and j_z to characterize the core state, thereby assuming that the atomic description remains valid for the initial one-electron state, even in a solid. Neglecting the magnetic or exchange field (and afterwards using first-order perturbation theory to get the splitting of the core states), the core-state wave function is expressed in terms of a radial function and spherical harmonics,

$$\psi_{nl_i j j_z}(\mathbf{r}, s) = \sum_{m_i} (-1)^{l_i + j_z - 1/2} \sqrt{2j + 1} \begin{pmatrix} l_i & 1/2 & j \\ m_i & s & -j_z \end{pmatrix} w_{nl_i j s}(r) Y_{l_i m_i}(\tilde{\mathbf{r}}). \quad (1.66)$$

The final one-electron state is a Bloch state characterized by the wave vector κ in the first Brillouin zone and the band index ν . In contrast to the initial state, the final-state

wave function is completely delocalized over the crystal. However, when calculating the matrix element in eq. 1.65, the strong localization of the core electron effectively cuts off the integral of their product at a finite radius. So one needs a description of the Bloch-electron only within that sphere since the overlap of initial and final states vanishes outside of that sphere. We expand the Bloch state in spherical harmonics and radial APW functions $u_{ls}^{E_{\kappa\nu}}(r)$. These functions are solutions inside the chosen sphere of the radial Schrödinger equation containing the spherical component of the crystal potential and the energy $E_{\kappa\nu}$ of the final state as eigenenergy, according to Slater's APW approach [57]. Thus the final state $\kappa\nu$ is given as

$$\Psi_{\kappa\nu}(\mathbf{r}, s) = \sum_{lm} d_{lms}^{\kappa\nu} u_{ls}^{E_{\kappa\nu}}(r) Y_{lm}(\tilde{\mathbf{r}}). \quad (1.67)$$

We now introduce the cross-density of states :

$$D_{lms}^{l'm's'}(E) = \sum_{f \equiv \kappa\nu} d_{lms}^f (d_{l'm's'}^f)^* \delta(E_f - E). \quad (1.68)$$

As the functions $u_{ls}^{E_{\kappa\nu}}$ are normalized, the modulus squared of the expansion coefficients $d_{lms}^{\kappa\nu}$ directly gives the contribution of this particular Bloch state to the local partial l, m -DOS, which is a diagonal term of the cross-DOS in eq. 1.68.

The interaction potential has to be expanded in a similar way as the wave functions. We utilize the Rayleigh formula for the exponential factor in terms of spherical Bessel functions j_λ :

$$e^{i\mathbf{q}\mathbf{r}} = 4\pi \sum_{\lambda=0}^{\infty} \sum_{\mu=-\lambda}^{+\lambda} i^\lambda Y_{\lambda\mu}(\tilde{\mathbf{q}})^* Y_{\lambda\mu}(\tilde{\mathbf{r}}) j_\lambda(qr). \quad (1.69)$$

To treat the remaining (relativistic) factor of the interaction potential, we write the impuls operator $\mathbf{p} = -i\hbar\nabla$ in a basis of spherical harmonics. The laboratory coordinate frame is fixed such that its z -axis is parallel to the beam and hence to \mathbf{v}_0 . In that case we need only retain the z -component of the impuls operator.

$$1 - (m_e c^2)^{-1} \mathbf{v}_0 \cdot \mathbf{p} = \sum_{lm} |lm\rangle \langle lm| - (m_e c^2)^{-1} i\hbar v_0 \sum_{lm} \left[\cos\theta |lm\rangle \frac{\partial}{\partial r} - m \frac{\cos\theta}{r} |lm\rangle - \sin\theta \frac{e^{-i\phi}}{r} \sqrt{(l-m)(l+m+1)} |lm+1\rangle \right] \langle lm| \quad (1.70)$$

Inserting eqs. 1.66 – 1.70 into eq. 1.65, we see that in the expanded matrix element $\langle i|V|f\rangle$ the radial and angular integration have been separated. The angular integrals

can be solved by using basic properties of the spherical harmonics and the Wigner $3j$ -symbols. We introduce the notation

$$\begin{aligned} \int d\Omega Y_{l_1 m_1}^* Y_{l_2 m_2} Y_{l_3 m_3} &= (-1)^{l_1 - m_1} \sqrt{\frac{[l_1 l_2 l_3]}{4\pi}} \begin{pmatrix} l_1 & l_2 & l_3 \\ -m_1 & m_2 & m_3 \end{pmatrix} \begin{pmatrix} l_1 & l_2 & l_3 \\ 0 & 0 & 0 \end{pmatrix} \\ &=: \left\{ \begin{matrix} l_1 & l_2 & l_3 \\ -m_1 & m_2 & m_3 \end{matrix} \right\}. \end{aligned} \quad (1.71)$$

Round brackets denote a Wigner $3j$ -symbol, curly brackets the product of three spherical harmonics.

The sum over initial states in eq. 1.65 is a sum over the quantum number j_z (we assume that we are interested in one particular core state (n, l_i, j) , and that all other core states give rise to transitions with an energy loss much different from that of the current edge), and the sum over final states is a sum over all Bloch states $\kappa\nu$. We obtain our main result:

$$\begin{aligned} \text{DFF}(\mathbf{q}, E) &= (4\pi)^2 \sum_{m_i m'_i} \sum_{l m s} \sum_{l' m' s'} \sum_{\lambda \mu} \sum_{\lambda' \mu'} \\ &D_{l m s}^{l' m' s'}(E + E_i) i^{\lambda - \lambda'} Y_{\lambda' \mu'}^*(\Omega_{\mathbf{q}}) Y_{\lambda \mu}(\Omega_{\mathbf{q}}) t_{l m s}^{\lambda \mu m_i} (t_{l' m' s'}^{\lambda' \mu' m'_i})^* \end{aligned} \quad (1.72)$$

$$\begin{aligned} t_{l m s}^{\lambda \mu m_i} &= \sum_{j_z} (-1)^{m_i + m'_i} (2j + 1) \begin{pmatrix} l_i & 1/2 & j \\ m_i & s & -j_z \end{pmatrix} \begin{pmatrix} l_i & 1/2 & j \\ m'_i & s' & -j_z \end{pmatrix} \\ &\times \left[\left\{ \begin{matrix} \lambda & l_i & l \\ -\mu & m_i & m \end{matrix} \right\} \int j_\lambda u_{ls} w_{nl_i j s} \right. \\ &+ \frac{i\hbar v_0}{m_e c^2} 2\sqrt{\frac{\pi}{3}} \int j_\lambda w_{nl_i j s} \left(\frac{\partial u_{ls}}{\partial r} - \frac{m}{r} u_{ls} \right) \\ &\times \left(\left\{ \begin{matrix} l+1 & l & 1 \\ -m & m & 0 \end{matrix} \right\} \left\{ \begin{matrix} \lambda & l_i & l+1 \\ -\mu & m_i & -m \end{matrix} \right\} \right. \\ &+ \left. \left\{ \begin{matrix} l-1 & l & 1 \\ -m & m & 0 \end{matrix} \right\} \left\{ \begin{matrix} \lambda & l_i & l-1 \\ -\mu & m_i & -m \end{matrix} \right\} \right) \\ &- \frac{i\hbar v_0}{m_e c^2} 2\sqrt{\frac{2\pi}{3}} \sqrt{(l-m)(l+m+1)} \int j_\lambda u_{ls} \frac{w_{nl_i j s}}{r} \\ &\times \left(\left\{ \begin{matrix} l+1 & l & 1 \\ -m+1 & m & -1 \end{matrix} \right\} \left\{ \begin{matrix} \lambda & l_i & l+1 \\ -\mu & m_i & -m+1 \end{matrix} \right\} \right. \\ &+ \left. \left. \left\{ \begin{matrix} l-1 & l & 1 \\ -m+1 & m & -1 \end{matrix} \right\} \left\{ \begin{matrix} \lambda & l_i & l-1 \\ -\mu & m_i & -m+1 \end{matrix} \right\} \right) \right] \end{aligned} \quad (1.73)$$

The indices lms and $l'm's'$ are related to the DOS. They allow the interpretation of the scattering cross section in terms of s-, p-, d-, and f-transitions. Spherical harmonics of order $\lambda\mu$ and $\lambda'\mu'$ describe the sample to beam orientation. The sample is rotated in the microscope, then the coordinate system in which the partial DOS is defined (called the crystal frame) and the laboratory frame rotate away from each other. Hence \mathbf{q} and $Y_{lm}(\mathbf{q})$ have to be rotated into the crystal frame (or, equivalently, the DOS has to be transformed to the laboratory frame). This is the origin of orientation sensitivity in equations 1.72 and 1.73.

Although eq. 1.72 contains apparently unrestricted summations over many indices, only a selected set of terms will contribute. The properties of the Wigner $3j$ symbols act as selection rules, eg. for $\lambda = 0$ the only allowed nonrelativistic term is the one that has $l = l_i$. Additionally, the radial integrals may make certain transitions very unfavorable. For $\lambda = 0$ and small scattering angles, one can approximate the spherical Bessel function j_λ by a constant, and the first radial integral in eq. 1.73 reduces to a product of initial and final state wave function, which is zero for $l = l_i$. So, terms for $\lambda = 0$ are not expected to contribute in this case.

The DDSCS is obviously "q-dependent". At a given energy loss, this means that the cross section depends on the scattering angle. In an EELS experiment one always has a finite collection semiangle (the angular width of the detector aperture) and convergence semiangle (the width of the beam). These parameters allow a certain range of wave vectors \mathbf{k} and \mathbf{k}' that, together with the energy loss E , determine a set of allowed \mathbf{q} . To simulate the experiment, one needs to integrate eq. 1.72 over this set of allowed \mathbf{q} -vectors.

Descriptions of ELNES are often limited to terms proportional to the DOS – that is, cross-DOS terms for which $l \neq l'$, $m \neq m'$ or $s \neq s'$ are not taken into account. In general, there is no reason for these "cross terms" to be zero. One can show that symmetry reduces the number of contributing cross terms [38]. For atoms with at least orthorhombic site symmetry, all cross terms disappear if the crystal frame is chosen accordingly.

For the simulation of ELNES for isotropic or polycrystalline specimens eq. 1.72 is simplified by integrating over all orientations of the scattering vector \mathbf{q} . This yields:

$$\text{DFF}(q, E) = \sum_{m_i m'_i} \sum_{lms} \sum_{l'm's'} D_{lms}^{l'm's'}(E + E_i) t_{lms}^{\lambda\mu m_i} (t_{l'm's'}^{\lambda'\mu' m'_i})^*. \quad (1.74)$$

Equations 1.72 and 1.73) can be easily reduced to the nonrelativistic case. It is sufficient to replace the speed of light c by infinity, and one immediately recovers the results of [38] and [19].

Working in the non relativistic case all cross terms cancel from eq. 1.74. In the relativistic case, however, eq. 1.73 shows that cross terms may still appear in the orientation averaged spectrum.

1.7.7 X-ray emission and absorption spectra (XES, XAS)

The formalism for the calculation of X-ray emission spectra within the APW was developed by Neckel et al. [36] and was later applied to the calculation of various systems [35].

According to Mohn [32] the number of transitions per given time from an initial to a final state can be derived from Fermi's golden rule and are given by

$$w_{a \rightarrow b}^{(-)} = \left(\frac{2\pi e}{m\hbar\omega} \right)^2 \frac{I}{c} | \langle b | e^{-i\vec{k}\vec{R}} \vec{e}\vec{P} | a \rangle |^2 \quad (1.75)$$

if $w_{ba} = \frac{1}{\hbar} (E_a^0 - E_b^0) > 0$.

The operator $e^{-i\vec{k}\vec{R}}$ for X-ray emission and absorption is of such a small value that it can be expanded into the Taylor series

$$e^{-i\vec{k}\vec{R}} = 1 + i\vec{k}\vec{R} - k^2 R^2 + \dots \quad (1.76)$$

Thus the matrix element is given by

$$\langle b | \vec{e}\vec{P} | a \rangle \approx \vec{e} \langle b | \vec{P} | a \rangle \approx i\omega_{ba} m \langle b | \vec{R} | a \rangle \quad (1.77)$$

In this matrix element the "electric dipole operator" \vec{R} is utilized and is therefore called the "dipole approximation".

To calculate the intensity of such a transition the following formula can be used:

$$I_{nk\sigma}(\nu) = \frac{8\pi e^2 (2\pi\nu)^3}{3\hbar c^3} \sum_l M_p(l, n'l', E)^2 W_{l,l'} \chi_l^P(E) \delta_{\sigma, \sigma_c} \quad (1.78)$$

where $M_p(l, n'l', E)^2$ is the radial transition probability given by

$$M_p(l, n'l', E) = \int_0^\infty R_{n,l}(r) R_{n',l'}(r) r^3 dr, \quad (1.79)$$

χ_l^P is the partial density of states of character l for atom P and $W_{l,l'}$ are weight factors for the angular integrals (containing the dipole selection rule $\Delta l = \pm 1$) and are given by

$$W_{l,l'} = \left(\frac{l+1}{2l+1} \right) \delta_{l,l'-1} + \left(\frac{l}{2l+1} \right) \delta_{l,l'+1} \quad (1.80)$$

This equation has been implementend into WIEN2k in the module txspec (see 2.2).

1.8 Broadening of spectra

The formulae given in the previous chapter yield the theoretical, unbroadened spectra of ELNES or XANES. Due to various physical processes, which are described in detail below, the features of these spectra are broadened. In earlier calculations using the Lorentz routine of the program `xspec` we only broadened emission spectra as described below. Recent works, however, have shown that the same formalism can also be applied to absorption spectra [59, 33]. This generalized broadening procedure is now implemented in WIEN2k in the module `broadening` (see 2.5).

There are mainly two effects that are responsible for the broadening of spectra.

1.8.1 Broadening of the core state

The broadening of core states is called “life-time broadening”. The core hole created by the excitation process is quickly filled (mainly by Auger processes, i.e. electrons from an energetically higher lying state fill up the hole, and the energy difference is transferred to another electron that is lifted into an unoccupied state). The finite life-time of the core hole gives rise to the broadening of the spectrum which depends on the type of the target atom. Life-time broadening is assumed to be constant and denoted with Γ_0 . Values for the life-times of core states are tabulated [44]. In the calculation we fold the theoretical spectrum with a Lorentzian with a halfwidth of Γ_0 .

1.8.2 Broadening of valence states

There are two processes that broaden valence states:

- the hole in the valence region is filled by an electron of higher energy. The energy difference can be used to excite another electron from the valence band into an unoccupied state.
- the radiationless transition of an electron to the core hole by an Auger process. Simultaneously two electrons from the valence band are scattered, one into the core and the other in a state above the Fermi level.

Emission spectra

Both effects contribute to the so called “low energy tailing” and is commonly described by the following equation:

$$\Gamma_{valence}(E) = W \left(1 - \frac{E - E_0}{E_F - E_0} \right)^2 \quad (1.81)$$

where W is the energy dependent broadening parameter, E_F the Fermi energy and E_0 the bottom energy of the lower band.

For emission spectra a “two-band broadening” scheme is implemented. This is necessary to properly describe the broadening of semicore states. We apply the formula for two different energy ranges, assuming that the broadening parameter W is the same for both band ranges.

Thus the formulae used for the broadening due to core **and** valence life-times can be written as:

$E_0 < E \leq E_F$	$\Gamma(E) = \Gamma_0 + W \left(1 - \frac{E-E_0}{E_F-E_0}\right)^2$
$E_1 < E \leq E_0$	$\Gamma(E) = \Gamma_0 + W$
$E_2 < E \leq E_1$	$\Gamma(E) = \Gamma_0 + W + W \left(1 - \frac{E-E_2}{E_1-E_2}\right)^2$
$E \leq E_2$	$\Gamma(E) = \Gamma_0 + 2W$

The broadening is implemented by folding the calculated spectrum with a Lorentzian according to the following equation:

$$I_1(E) = I_0(E) - \frac{1}{\pi} \frac{\Gamma(E)}{(E - E_i)^2 + \Gamma(E)^2} \quad (1.82)$$

Absorption spectra

For absorption spectra two different formulae are implemented. One scheme using a similar formula as in the emissions part, given by Muller et al. [34] which is derived from the random phase approximation (RPA):

$$\Gamma = \frac{\pi^2 \sqrt{3}}{128} \omega_{plasma} \left(\frac{E}{E_0}\right)^2 \quad (1.83)$$

where E_0 is the bottom of the valence band and ω_{plasma} the plasma frequency.

The other scheme is an empirical linear function described by Weijs et al. [59] where the broadening parameter assumes the following form:

$$\Gamma(E) = \Gamma_0 + \frac{E}{10} \quad (1.84)$$

1.8.3 Instrumental broadening

The instrumental broadening is included by folding the simulated spectrum with a Gaussian function with a FWHM corresponding to the energy resolution of the actual spectrometer that was used in the experiments.

1.9 The Core Hole

The process giving rise to (core level) electron energy loss spectra or X-ray absorption spectra includes the excitation of a core electron into an unoccupied state leaving an electron hole in the core region. This core hole gives rise to a modified potential acting on the other electrons. In this section we describe briefly how this core hole can be taken into account (or be neglected).

1.9.1 Initial State Approximation

In earlier calculations the effects of the core hole were neglected completely. For many systems even a regular ground state calculation is sufficient. We call this the "initial state approximation".

1.9.2 Final State Approximation

Despite the good agreement of the "initial state approximation" for many systems, various authors have shown, that some systems require the inclusion of a core hole in the simulation in order to arrive at reasonable spectra (see e.g. [11, 59, 12, 27, 8, 28, 10] and many more).

In the final state approximation we create a core hole of infinite life time, which in due course results in a modified potential, which is taken care of in the SCF cycle, relaxing the other electrons in the presence of the core hole. Often this approximation overestimates the effect of the real core hole by far. This is due to the fact that we artificially (by the periodic boundary conditions) create interactions between the core hole site and its next periodic image. In order to reduce this artificial core hole – core hole interaction, we can perform this approach in a supercell and thus reduce this unphysical interaction by enlarging the distance between the periodic images. This makes the effect of the core hole on the crystal potential much smaller and more realistic.

1.9.3 Partial Core Hole Screening (PCS)

As both the initial state approximation and the final state approximation are static descriptions of the inherently dynamic process of exciting a core electron to an unoccupied state, we recently developed a method which lies in between and allows us to model the time-dependent excitation process in a static description [29].

The idea behind the PCS is that in real systems the core hole will be screened by (free) valence electrons. The electrons screening the core hole create a different potential on the site, which in due course also changes the wavefunctions and thus the resulting spectrum.

In the PCS we introduce a fractional occupation number at the atom which hosts the core hole. In doing so we can vary between initial state (no electrons missing) and final state approximation (1.0 electron missing). This allows us to adjust the simulated result to the experimental spectrum in order to optimize the PCS value.

1.9.4 Slater's Transition State

Density Functional Theory is by definition limited to the calculation of ground states. Energy eigenvalues derived from an SCF calculation should not be mistaken as excitation energies. However, many experiments show, that DFT gives at least a good estimate, even for properties involving electronically excited states such as absorption spectra. However the excitation energy is not directly accessible using a standard calculation. These energies can be calculated by either performing two calculations (ground state and excited state) and taking the mean value, or by performing one calculation involving Slater's Transition State [58], which is equivalent to a partial core hole of 0.5 electrons.

1.9.5 Beyond these simple concepts . . .

Since I began my work on electron energy loss spectra, there have been many new developments. Today new codes or addition to codes appear that implement concepts that are better suited for the description of excited states than standard DFT. These include e.g. the response based method of time dependent DFT, perturbational methods like GW or the Bethe-Salpeter equation or the density matrix approach. Furthermore there is work going on in the improvement of ground state calculations by implementing Exact Exchange functionals. However, none of these have been utilized in the work presented here, because at the time of performing the calculations they were not available.

Programs

*Program complexity grows until it exceeds
the capability of the programmer who must maintain it.*
from Murphy's Laws

2 Programs

2.1 WIEN2k

In this work the calculations were performed with the program package WIEN2k [4]. This program package for the calculation of electronic properties of crystals is an implementation of the (L)APW+lo method (see 1.5) and is based on the original WIEN code [6].

The program package was developed over the past 25 years by Karlheinz Schwarz and Peter Blaha and many co-workers. At present it is used by more than 900 groups all over the world.

In the following section the different parts of the program package will be briefly described. An extended description can be found in [51, 50] and in the user's guide [4].

2.1.1 Introduction

The program package WIEN2k consists of a number of programs that are linked together with csh shell-scripts and features a web-based graphical interface called w2web. The programs are mainly written in FORTRAN90. Only a few utility programs were written in C. There are many utilities and scripts included to simplify the work with the package, partly as csh-shell or as perl scripts.

2.1.2 Input

In principle ab-initio programs would only require the knowledge of the nuclear charge of the atoms involved. In practice at least the crystal structure is needed to arrive at a solvable problem.

During the initialization process WIEN2k generates a number of input files for the different programs. For very simple cases it is sufficient to use the pre-selected default values. However, for more sophisticated problems it is possible to vary certain parameters, such as e.g. the occupation number of core states, which will be necessary for the calculation of spectra with a core hole, as will be described later.

2.1.3 Initialization

Before a calculation can be started an initial electron density has to be known in order to calculate the potential. During this setup phase the following programs are run:

- nn** calculates the distances of the nearest neighbors and tests for overlapping spheres. It also generates a shell structure which can be useful for constructing supercells.
- sgroup** determines the spacegroup as well as all pointgroups of non-equivalent sites. It produces a proper `case.struct` file if necessary.
- lstart** solves the Schrödinger (Dirac) equation for the free atoms and calculates their electron densities.
- symmetry** generates the symmetry operations for the given atomic position and crystal structure, it further determines the point group of the atomic positions and generates the corresponding LM combinations for the lattice harmonics (see 1.5.5).
- kgen** generates a k-mesh in the irreducible part of the Brillouin zone.
- dstart** calculates a starting density by superposition of electron densities with the crystal density.

2.1.4 SCF cycle

In the SCF cycle the calculation is repeated until given convergence criteria are met. During the SCF cycle the following programs are executed:

- lapw0** calculates the total potential V_{tot} as the sum of Coulomb V_{coul} and exchange correlation potential V_{xc} (see 1.5.5), which are generated from the input density.
- lapw1** calculates Hamilton- and overlap matrix elements. By diagonalizing the general eigenvalue problem the eigenvectors and energy eigenvalues are calculated. To speed up the calculation an (optional) iterative diagonalization is implemented.
- lapw2** calculates the Fermi level and the valence charge density from Kohn-Sham orbitals specified by the the eigenvectors.
- lcore** calculates the eigenvalues and charge-densities for the core states.
- mixer** calculates the total electron density from the core and valence states for the following cycle. The output density is mixed with the old input density using the Pratt or Broyden-II scheme to ensure convergence during the SCF cycle.

For a schematic drawing of the SCF cycle see fig. 2.1.

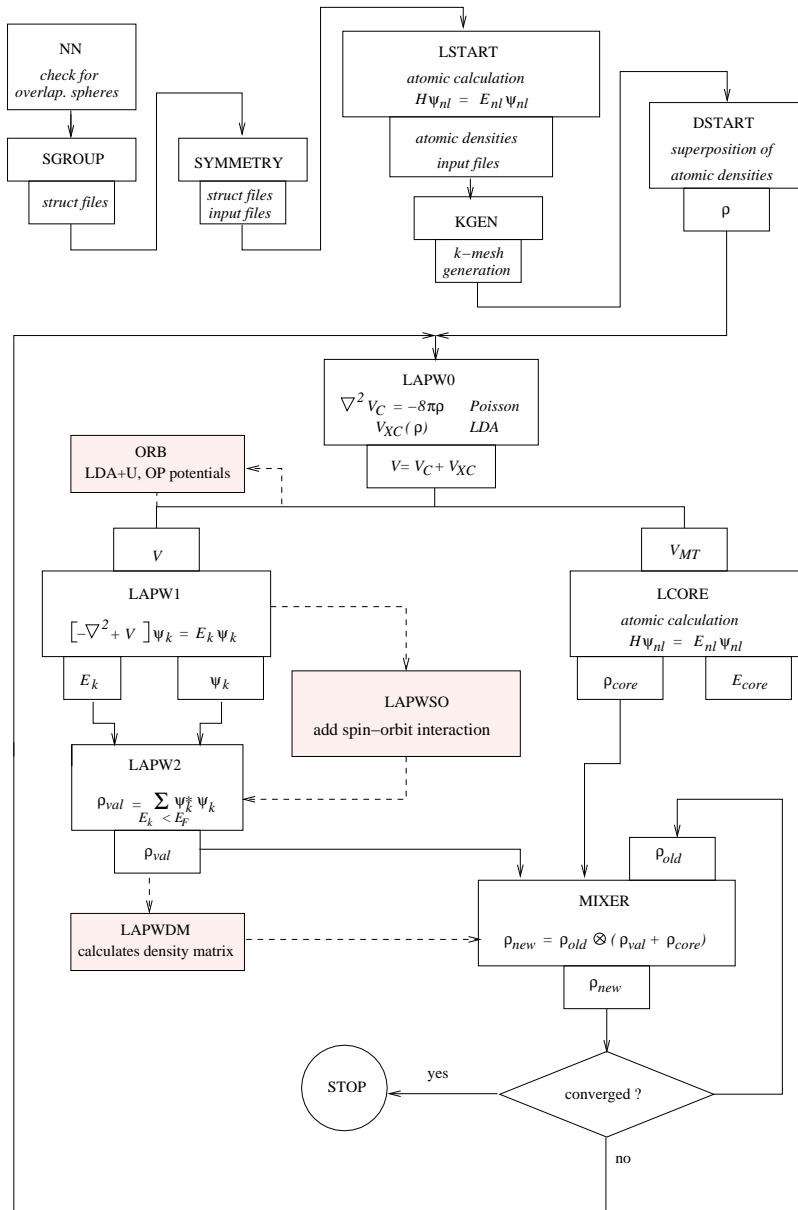


Figure 2.1: Schematic drawing of the SCF-cycle in WIEN2k

2.2 XSPEC

With `xspec` it is possible to calculate both emission and absorption X-ray near edge structures depending on the input. It is strictly limited to dipole allowed transitions.

This module consists of four programs which are linked by a csh-script which is itself called `xspec`. These programs are

initxspec generates the input file (`case.int`) for the subsequent run of the program `tetra`; the input is chosen such that the partial DOS for the $L + 1$ and the $L - 1$ contributions (for edges higher than K) are calculated.

tetra calculates the partial DOS

txspec uses the generated partial DOS and multiplies them with the radial transition probability derived from eq. 1.79 and the transition matrix elements according to eq. 1.80. This step is done for both the $L + 1$ and the $L - 1$ contribution to the spectrum (intermediate results can be found in the files `case.m1` for the $L + 1$ component and in `case.m2` for $L - 1$) and finally both are added to yield the theoretical spectrum. It should be noted, that the program automatically selects core states with the spin $s = +1$ (i.e. $p_{3/2}$ or $d_{5/2}$ states) and thus yields only L_{III} or M_V spectra.

lorentz to compare the theoretical spectra obtained by `txspec` one has to broaden the spectra to account for lifetime effects and the finite resolution of the spectrometer. Life-time broadening of core states is introduced by folding the spectrum with a Lorentzian of fixed FWHM. For the lifetime of the valence states an energy-dependent Lorentzian is chosen; in the current implementation of `lorentz` valence-broadening is only applied in the case of emission spectra. Finally spectrometer broadening is introduced by folding the obtained spectrum with a Gaussian of constant FWHM. The original `lorentz` program was later improved and extended, which is described in section 2.5, where also a detailed description of the formulae used for broadening is given.

In order to use this module, self consistent results are indeed needed.

2.3 ELNES

Note: *ELNES is no longer part of the WIEN2k distribution. It has been replaced by TELNES.2. Nonetheless we describe it here because the simulations presented in this thesis were performed using this program module. The results presented here can be reproduced using TELNES.2 by turning off the relativistic correction.*

The module `e1nes` is used for the calculation of electron energy-loss near edge structures (ELNES). In contrast to `xspec` it also includes non-dipole contributions and is further able to calculate orientation dependent spectra.

Much like `xspec` it is a set of programs linked by the script `elnes`, which connects the following programs:

initelnes generates the input file (`case.int`) for the subsequent run of the program `tetra`. It should be noted that for orientation dependent spectra the partial DOS must be split into lm contributions when using eq. 1.63 (generated by setting `ISPLIT=88` in `case.struct`) or into the called cross-DOS (see [37]) when using eq. 1.64 (by setting `ISPLIT=99`).

tetra calculates the partial DOS

telnes calculates the electron energy loss spectrum according to eq. 1.62 for polycrystalline samples, or for orientation dependent spectra according to eq. 1.63. For highly anisotropic samples (i.e. with symmetries lower orthorhombic) the calculation is done according to eq. 1.64. `telnes` includes a simple broadening routine, which corrects for finite instrumental resolution using a Gaussian with fixed FWHM. No life-time effects are included in this program. They can be applied by the program `broadening`

2.4 TELNES.2

Equations 1.72 and 1.74 as described in [21, 22] are implemented in the program `TELNES.2`, the successor of the `TELNES` module. The `TELNES.2` program is available as a module of the `WIEN2k` package. In this chapter we describe very briefly how certain ingredients for the DDSCS (see section 1.7.6) are calculated, and how the DDSCS itself is processed into a useful spectrum.

The radial APW basis functions u_{ls} and the core radial function w_{nljs} are calculated from the spherical part of the crystal potential given by `WIEN2k`.

As the `WIEN2k` code uses atomic spheres, and we limit our radial integrals to this sphere according to the discussion of eq. 1.67, care must be taken that the atomic sphere radius (ASR) is chosen large enough so that the initial and final state wave functions fulfill the appropriate orthogonality conditions inside the sphere. If this is not done, unphysical dependencies might occur in the DDSCS [16].

How the cross-DOS can be obtained from an LAPW calculation has been discussed earlier [19]. For the calculation of cross terms in the DOS, until now it was not possible to exploit the symmetry of the lattice to map the Brillouin zone onto its irreducible wedge. In collaboration with other `WIEN2k` developers [39] we have recently solved this problem, so that the full lattice symmetry can now be used. This can considerably speed up calculations.

In practice, one usually studies single differential cross sections. Therefore we offer the option to either integrate the DDSCS in eq. 1.72 over energy (and study the cross

section as a function of scattering angle or impuls transfer), or to integrate it over scattering angle, and obtain an energy differential cross-section.

In the latter case, we integrate over a collection and convergence angle numerically. In principle, the DDSCS should be integrated over the set of \mathbf{k} allowed by the convergence angle, and then again integrated over the set of \mathbf{k}' allowed by the collection angle. However, experimental conditions in the microscope restrict these angles to less than 50 mrad in all practical cases. The dependence of the cross section on sample to beam orientation is situated on a larger scale. A 50 mrad tilt of a crystal under the beam has practically no influence on the ELNES. We therefore do not integrate over the two \mathbf{k} -distributions separately, but only over the correlation of these two distributions, i.e. over a set of allowed \mathbf{q} .

Finally, the energy differential cross sections are broadened in three steps: Lorentzian broadening for the core hole life time; energy-dependent Lorentzian broadening for the final state life time; and Gaussian broadening to simulate all instrumental broadening processes.

All calculational parameters for the `telnes.2` program can be set in an intuitive way through the user interface `w2web` of WIEN2k (in regular mode only a limited set of input parameters are shown, however, there exists also an "ELNES expert more" in which all parameters can be set through the interface). The sample to beam orientation is defined by three Euler angles. Specific input options as well as detailed output facilitate interpretation of the spectrum, especially in terms of the l, m, s character of the final state. We also provide extensive documentation for both users and developers [20].

2.5 BROADENING

Since recently the broadening program is part of the WIEN2k distribution. It was derived from the `lorentz` program, which is part of the `xspec` package. However, the latter had a few short-comings. With `broadening` it is now possible to specify different smearing parameters for L_2 and L_3 spectra without using external programs. Furthermore a routine for broadening valence states in absorption mode has been added. Depending on the choice of input two variants of energy-dependent broadening of valence states can be utilized:

$E/10$ an empirical broadening, where $\Gamma = (E - E_F - W_{shift})/10$. By using W_{shift} this broadening can also be applied to systems containing a gap [59].

E^2 a broadening similar to the one applied to the emission spectra as described by Muller [34]. We implemented the following formula:

$$\Gamma = \frac{\pi^2 * \sqrt{3}}{128} * \omega_{plasma} * \left(\frac{E}{E_0}\right)^2$$

where E_0 is the bottom of the valence band and ω_{plasma} ($E1$ in the input file) the plasma frequency.

The version of broadening included now in WIEN2k can be used in conjunction with both the `xspec` and the `telnes2 telnes` packages.

Results

Prediction is very difficult,
especially about the future.
Niels Bohr

3 Results

Contents

3.1 Aluminum	49
3.1.1 Aluminum metal	49
3.1.2 Aluminum oxide	51
3.2 Magnesium	53
3.2.1 Magnesium metal	53
3.2.2 Magnesium oxide	54
3.3 Titanium	57
3.3.1 Titanium metal	57
3.3.2 Titanium oxide	59
3.4 Copper	61
3.4.1 Copper metal	61
3.4.2 Copper oxide	64

To investigate the effect of a (partial) core hole on the simulated ELNES, we selected a few materials for this work. The requirements for selection were as follows:

(1) the materials must consist of p- or d-elements to show the localisation of the final state, (2) metal and its oxide must be available for the investigation to show the difference between metallic and insulating behaviour, and (3) the edge must be accessible for analysis with TEM/EELS, i.e. less than 2000 eV.

Therefore the following systems were selected:

- Al metal and Al₂O₃ (Al-K edge at 1560 eV)
- Mg metal and MgO (Mg-K edge at 1305 eV)
- Ti metal and TiO₂ (Ti-L₂₃ edges at 456 and 462 eV)
- Cu metal and Cu₂O (Cu-L₂₃ edges at 931 and 951 eV)

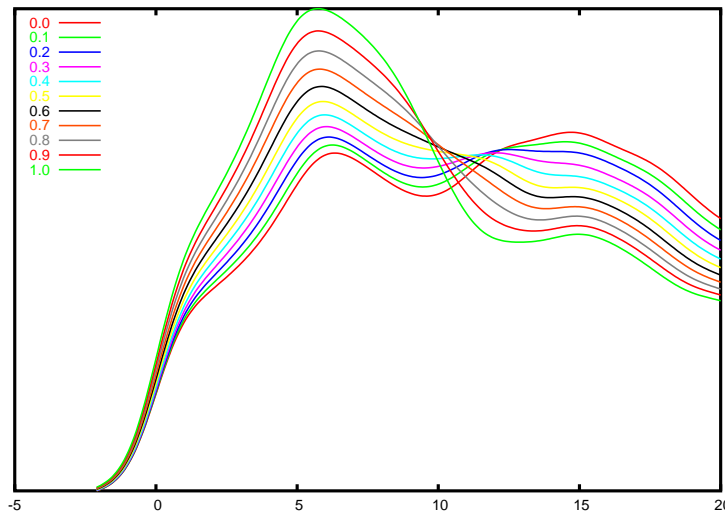


Figure 3.1: Partial core hole in the aluminum Al-K spectrum, varying the core hole from no (0.0) to a full missing electron (1.0)

For the systematic investigation of each system mentioned calculations with a partial core hole (from no to a full core hole in steps of 0.1 electrons) in the single cell were performed. For some systems also a $2 \times 2 \times 2$ supercell calculation with one full core hole was performed. For Al_2O_3 (a low symmetry structure) the supercell simulation could not be performed because of lack of computer time. For the Mg metal the $2 \times 2 \times 2$ supercell could not be converged. A much smaller mixing factor might have helped but that would have again required more CPU time than was available.

3.1 Aluminum

3.1.1 Aluminum metal

Metallic aluminum crystalizes in the cubic face centered space group $255 Fm\bar{3}m$ with lattice parameters of $a = b = c = 7.637$ Bohr. Computational parameters were 5000 k-points in the IBZ and a cut-off of $R_{mt} * k_{max} = 8.0$.

From figure 3.1 we see that the shoulder of the first peak is more pronounced if there is no core hole present. The first peak at approx. 6 eV increases in height whereas the second peak at approx. 15 eV decreases in height in the presence of a core hole.

Comparing the theoretical edge onset derived from the energy level of the aluminum $1s$ states shows, that the experimental value of 1560 eV is very close to the value derived for a partial core hole of 0.4.

PCH	$1s$ (Ry)	E_F (Ry)	Edge (Ry)	Edge (eV)
0,0	-110,18438	0,52520	110,71	1506,31
0,1	-111,15117	0,51560	111,67	1519,34
0,2	-112,12021	0,50531	112,63	1532,38
0,3	-113,11019	0,49304	113,60	1545,69
0,4	-114,08157	0,48135	114,56	1558,74
0,5	-115,05798	0,46878	115,53	1571,86
0,6	-116,02895	0,45593	116,48	1584,89
0,7	-117,00430	0,44219	117,45	1597,98
0,8	-117,97244	0,42808	118,40	1610,96
0,9	-118,94774	0,41245	119,36	1624,01
1,0	-119,90980	0,39685	120,31	1636,89

Table 3.1: Core levels and calculated K edge onset in aluminum with a partial core hole

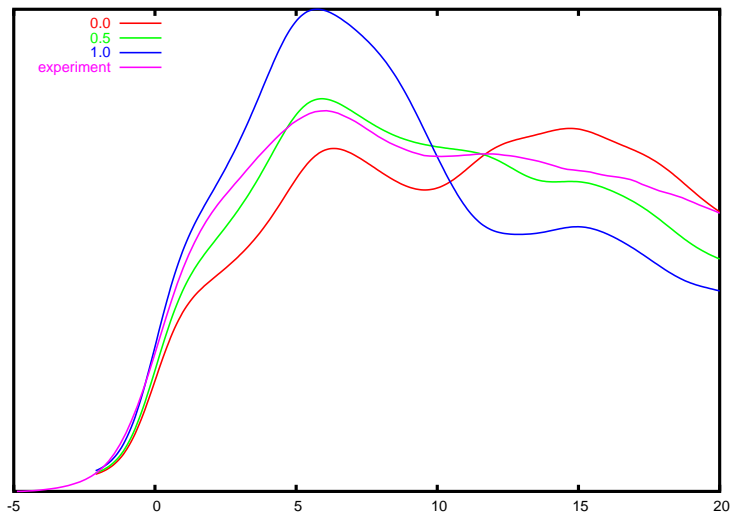


Figure 3.2: Al-K ELNES of aluminum metal with no, half and a full core hole, and the experimental spectrum

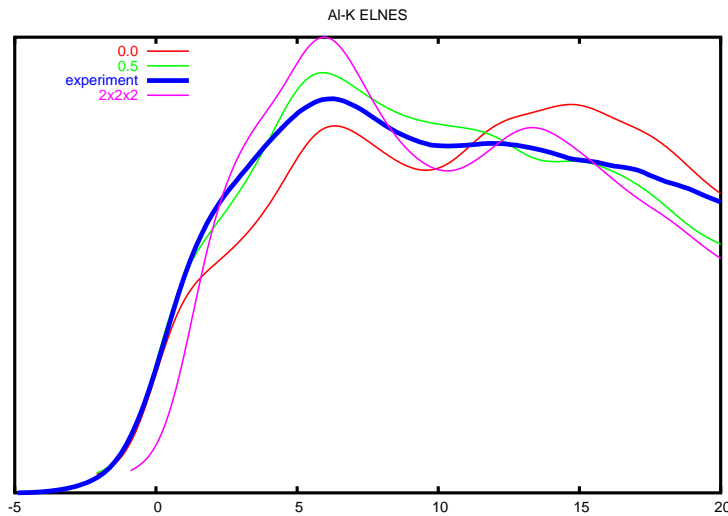


Figure 3.3: ELNES of the aluminum K edge in a 2x2x2 supercell and comparison with results from the single cell calculation (no and half core hole) as well as the experimental spectrum

The comparison of the Al-K ELNES of aluminum with no, half and a full core hole, and the experimental spectrum in figure 3.2 shows best agreement between experiment and simulation for half a core hole.

A 2x2x2 supercell was constructed with lattice parameters of $a = b = c = 15.274$ Bohr. The supercell simulation was performed with 1000 k-points in the IBZ and a cut-off parameter of $R_{mt} * k_{max} = 7.0$.

Figure 3.3 shows the comparison of the aluminum K edge in aluminum for the single cell (no and half core hole), the experimental spectrum und the spectrum for a 2x2x2 supercell with a full core hole. Here we clearly see that the supercell calculation would be favorable in respect to peak positions, but with regard to relative peak heights, the calculation using half a core hole is superior.

3.1.2 Aluminum oxide

Aluminum oxide Al_2O_3 in the form of corundum crystalizes in the rhombohedral space group 167 $R\bar{3}c$ with lattice parameters of $a = b = 8.989 \text{ \AA}$ and $c = 24.546 \text{ \AA}$. In the calculation a cut-off parameter of $R_{mt} * k_{max} = 8.0$ and 1500 k-points were used.

In figure 3.4 we see that the shoulder structure of the calculated Al-K ELNES disappears by introducing a (partial) core hole and the peak maximum shifts from approx. 17 eV for no core hole to approx. 12 eV for a full core hole.

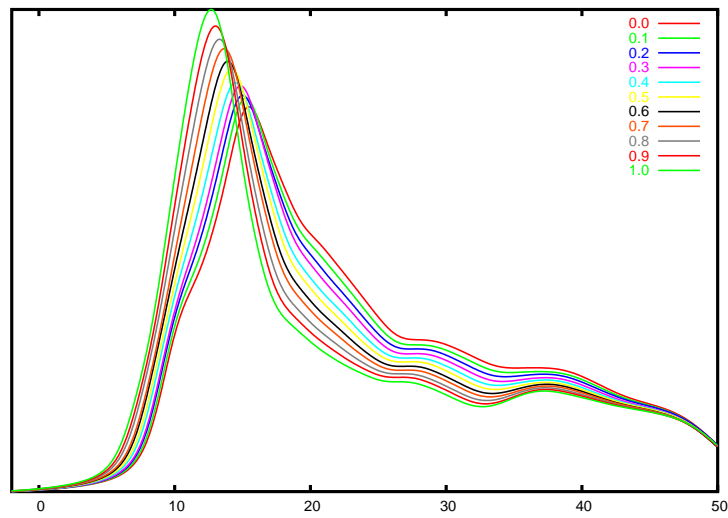


Figure 3.4: Partial core hole (0.0 to 1.0) in the Al-K ELNES for aluminum oxide

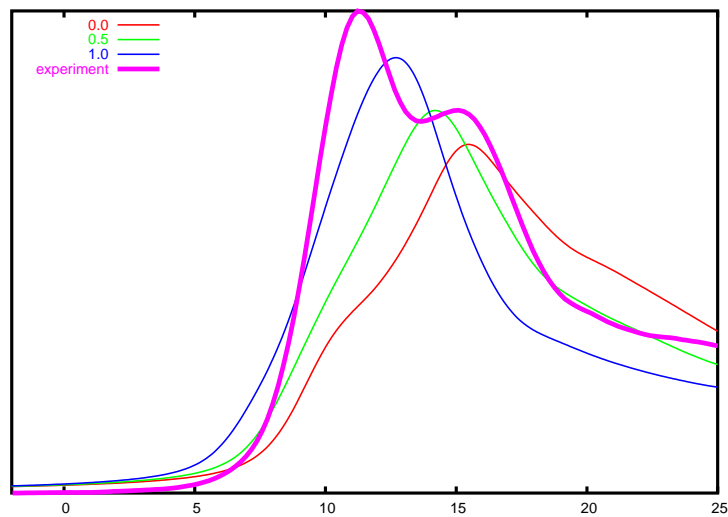


Figure 3.5: Al-K ELNES of aluminum oxide with no, half and a full core hole, and the experimental spectrum

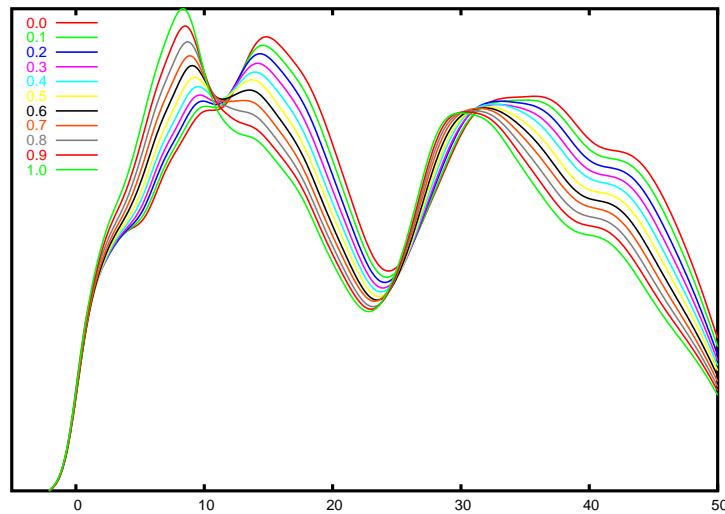


Figure 3.6: Partial core hole in the magnesium Mg-K spectrum, varying the core hole from no (0.0) to a full missing electron (1.0)

Figure 3.5 plots the calculated Al-K ELNES in aluminum oxide for no, half and a full core hole as well as the experimental spectrum. We see that the experiment exhibits a clear double peak structure, whereas the simulation can at best generate a shouldered structure in the case of no core hole. It seems that this system needs to be simulated in a supercell to get better agreement with the experiment. However simulating an aluminum oxide supercell would require much more CPU time than was available, as it has to be simulated in a low symmetry structure.

3.2 Magnesium

3.2.1 Magnesium metal

Metallic magnesium crystallizes in the hexagonal spacegroup $194 P6\bar{3}/mmc$, with lattice parameters of $a = b = 6.053$ Bohr and $c = 9.827$ Bohr. In the calculation we used 3000 k-points in the IBZ and a cut-off parameter of $R_{mt} * k_{max} = 8.0$.

As can be seen from figure 3.6, the shoulder of the spectrum is more pronounced if no core hole is present. Varying the core-hole from zero to a full electron, the first peak increases in height, whereas the second decreases by almost the same amount, thus giving equal peak heights for the case of half a core hole. The third peak height, however, is not affected in height but the position shifts by 5 eV towards lower energy with increasing core-hole strength. The fourth peak shifts by approx. 2 eV towards

PCH	$1s$ (Ry)	E_F (Ry)	Edge (Ry)	Edge (eV)
0,0	-92,03064	0,26304	92,29	1255,75
0,1	-92,89166	0,26050	93,15	1267,43
0,2	-93,76005	0,26914	94,03	1279,36
0,3	-94,62246	0,25434	94,88	1290,89
0,4	-95,49036	0,25104	95,74	1302,66
0,5	-96,35930	0,24761	96,61	1314,43
0,6	-97,22874	0,24369	97,47	1326,21
0,7	-98,09909	0,23935	98,34	1337,99
0,8	-98,96551	0,23484	99,20	1349,72
0,9	-99,82983	0,23007	100,06	1361,41
1,0	-100,69561	0,22438	100,92	1373,12

Table 3.2: Core levels and calculated K edge onset in magnesium with a partial core hole

lower energy and noticeably decreases its height drastically.

From these calculations the energy levels of the $1s$ states were extracted. Together with the Fermi level the theoretical edge onset could be calculated. The calculated value for the 0.4 partial core hole is very close to the experimental value of 1305 eV (see table 3.2.1).

In figure 3.7 a comparison of the Mg-K ELNES of magnesium with no, half and a full core hole, and the experimental spectrum is shown. As is readily visible the calculated spectrum without core hole resembles the experimental spectrum best. Introducing even a partial core hole cannot reproduce the first part of the spectrum.

3.2.2 Magnesium oxide

Magnesium oxide crystallizes in a face centered cubic structure, space group $Fm\bar{3}m$, with $a = b = c = 7.962$ Bohr. In the calculation 5000 K-points in the IBZ and a cut-off parameter of $R_{mt} * k_{max} = 8.0$ were used.

Figure 3.8 shows that the shoulder of the main peak in the ELNES of MgO is less pronounced in the calculation with a core hole, but still visible as a shoulder. The main peak shifts by 3 eV to lower energy with a full in comparison to no core hole. The second peak shifts by approx. 2eV and is almost completely suppressed in the presence of the core hole.

Comparing the Mg-K ELNES of magnesium oxide with no, half and a full core hole, and the experimental spectrum in figure 3.9 one immediately sees, that the shoulder in the simulated spectra is a separated peak in the experiment.

In figure 3.10 the ELNES of a the $2 \times 2 \times 2$ supercell is shown together with the exper-

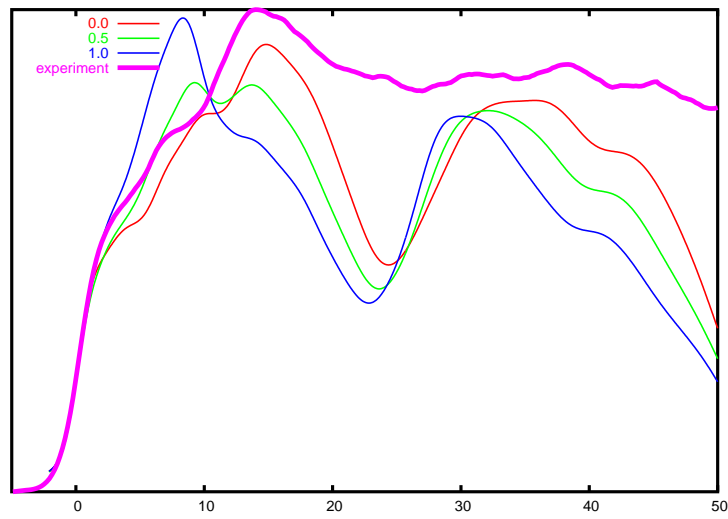


Figure 3.7: Mg-K ELNES of magnesium metal with no, half and a full core hole, and the experimental spectrum

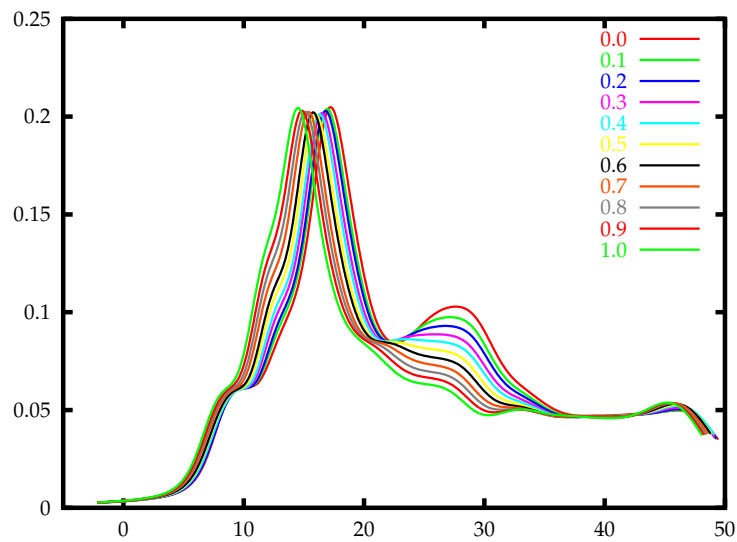


Figure 3.8: Partial core hole in the Mg K ELNES in magnesium oxide, varying the core hole from no (0.0) to a full missing electron (1.0)

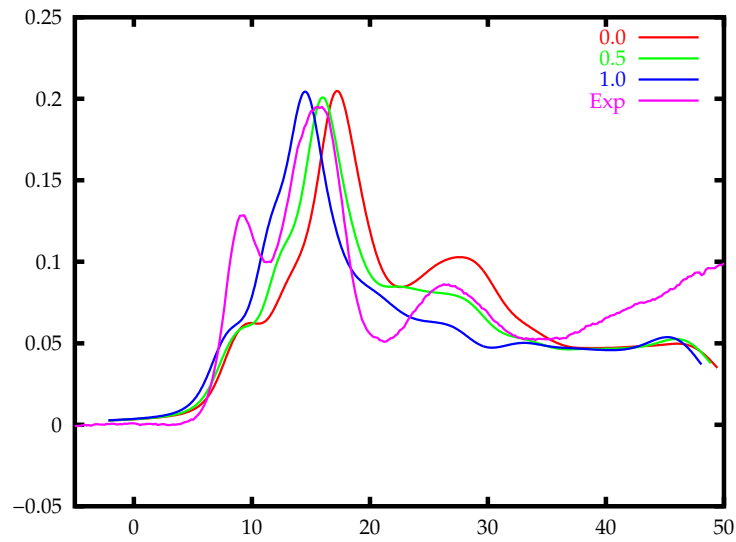


Figure 3.9: Mg-K ELNES of magnesium oxide with no, half and a full core hole, and the experimental spectrum

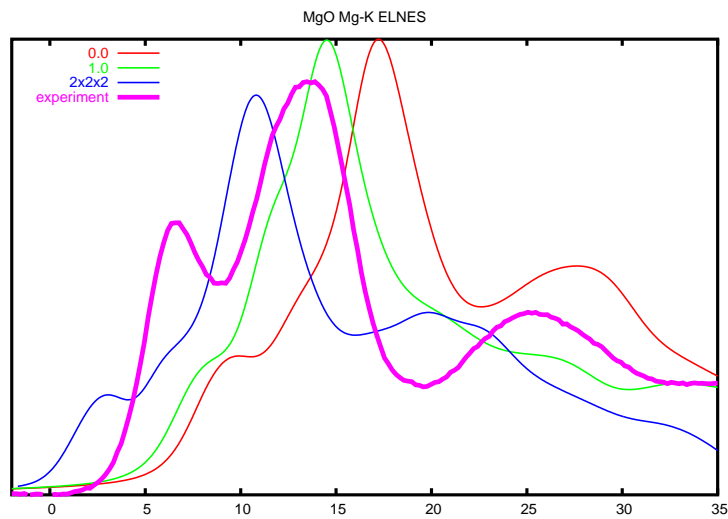


Figure 3.10: Mg-K ELNES of magnesium oxide in a 2x2x2 supercell with full core hole in comparison with the experiment and a single cell with no and a full core hole

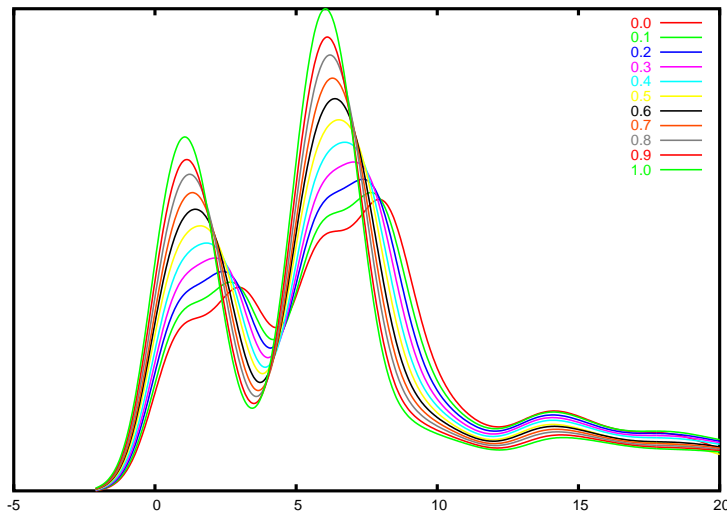


Figure 3.11: Partial core hole in the titanium Ti- L_3 ELNES, varying the core hole from no (0.0) to a full missing electron (1.0)

imental spectrum and the comparison with corresponding spectra of the single cell with no and a full core hole. The experimental spectrum lies between the spectra of the single and the supercell with a full core hole, however, the first peak in the calculations is always much smaller than the experimental one.

3.3 Titanium

3.3.1 Titanium metal

Metallic titanium crystalizes in the space group $P\bar{6}_2m$. The lattice parameters are $a = b = 5.576$ and $c = 8.850$ Bohr. For the calculation a plane wave cut-off of $R_{mt} * k_{max} = 8.0$ and 3000 k-points were used.

From figure 3.11 we see a shouldered double peak structure in the calculated ELNES. The shoulders, which are not present in the experimental spectrum, disappears by introducing a (partial) core hole. From figure 3.12 we see that the relative peak heights of the experimental spectrum are best reproduced by a calculation with half a core hole.

From the calculations given in tables 3.3.1 and 3.4 the energy levels of the Ti L_2 and L_3 states were extracted. Together with the Fermi level the theoretical edge onset was calculated. The calculated values for the 0.5 partial core hole is very close the the experimental values of 456 eV for the L_2 and 462 eV for the L_3 edge of Ti.

PCH	$2p_{1/2}$ (Ry)	E_F (Ry)	Edge (Ry)	Edge (eV)
0,0	-31,41758	0,67139	32,09	436,60
0,1	-31,70357	0,65289	32,36	440,24
0,2	-31,98794	0,63413	32,62	443,86
0,3	-32,27068	0,61518	32,89	447,44
0,4	-32,55192	0,59589	33,15	451,01
0,5	-32,83177	0,57621	33,41	454,55
0,6	-33,10997	0,55633	33,67	458,06
0,7	-33,38639	0,63645	34,02	462,91
0,8	-33,66143	0,51619	34,18	465,02
0,9	-33,93495	0,49581	34,43	468,46
1,0	-34,20739	0,47523	34,68	471,89

Table 3.3: Core levels and calculated L_2 edge onset in titanium with a partial core hole

PCH	$2p_{3/2}$ (Ry)	E_F (Ry)	Edge (Ry)	Edge (eV)
0,0	-31,84177	0,67139	32,51	442,37
0,1	-32,12949	0,65289	32,78	446,04
0,2	-32,41621	0,63413	33,05	449,68
0,3	-32,70099	0,61518	33,32	453,30
0,4	-32,98428	0,59589	33,58	456,89
0,5	-33,26620	0,57621	33,84	460,46
0,6	33,54647	0,55633	34,10	464,00
0,7	-33,82496	0,63645	34,46	468,88
0,8	-34,10209	0,51619	34,62	471,02
0,9	-34,37771	0,49581	34,87	474,49
1,0	-34,65224	0,47523	35,13	477,94

Table 3.4: Core levels and calculated L_3 edge onset in titanium with a partial core hole

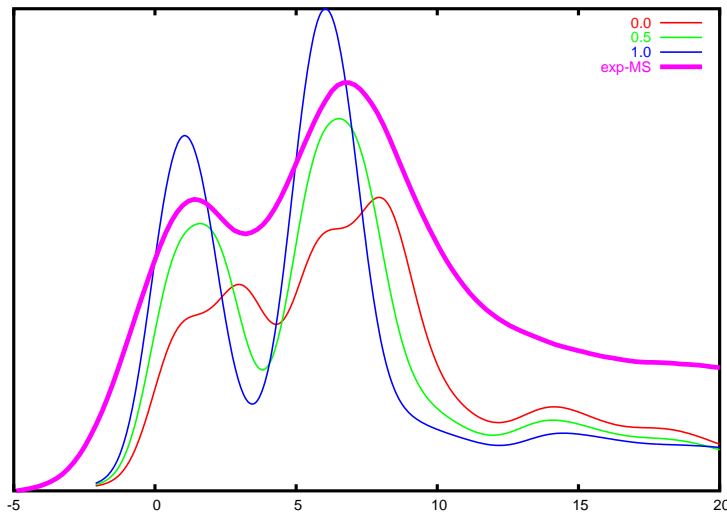


Figure 3.12: ELNES of titanium Ti- L_3 edge with no, half and a full core hole, and the experimental spectrum

3.3.2 Titanium oxide

Titanium oxide, TiO_2 as rutile crystalizes in the tetragonal space group $136 P4_2/mnm$ with lattice parameters of $a = b = 8.682$ Bohr and $c = 5.592$ Bohr. In the calculation a cut-off parameter of $R_{mt} * k_{max} = 8.0$ and 2500 k-points were used.

Figure 3.13 shows the effect of a (partial) core hole on the Ti- L_3 ELNES in titanium oxide. By increasing the core hole from 0.0 to 1.0 the spectrum shifts by approx. 2 eV towards the Fermi level. Except for a more and more pronounced shoulder on the first peak, the (partial) core hole does not influence other features in the spectrum.

In figure 3.14 we compare the experimental spectrum with the simulation for no, half and full core hole. The simulated spectra are generally too broad and cannot reproduce the relative peak heights.

From figure 3.15 we see that the supercell calculation with core hole can reproduce very well the width of the first peak, as well as the positions of the second and third. The relative peak heights, however, are not given correctly, just as in the simulation using the simple cell.

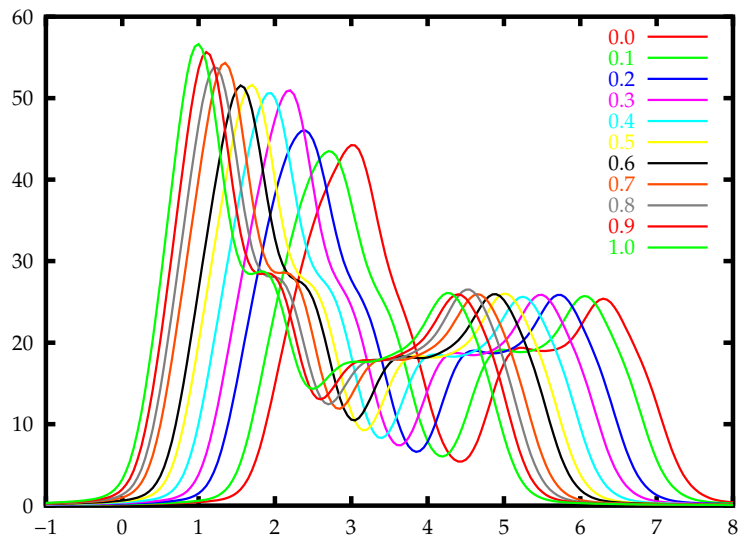


Figure 3.13: Partial core hole in Ti- L_3 ELNES of titanium oxide varying the core hole from no (0.0) to a full missing electron (1.0)

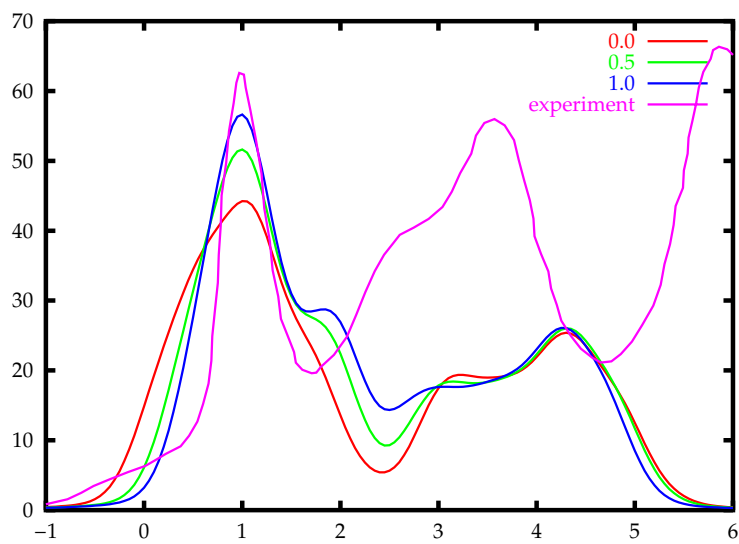


Figure 3.14: Ti- L_3 ELNES of titanium oxide with no, half and a full core hole, and the experimental spectrum

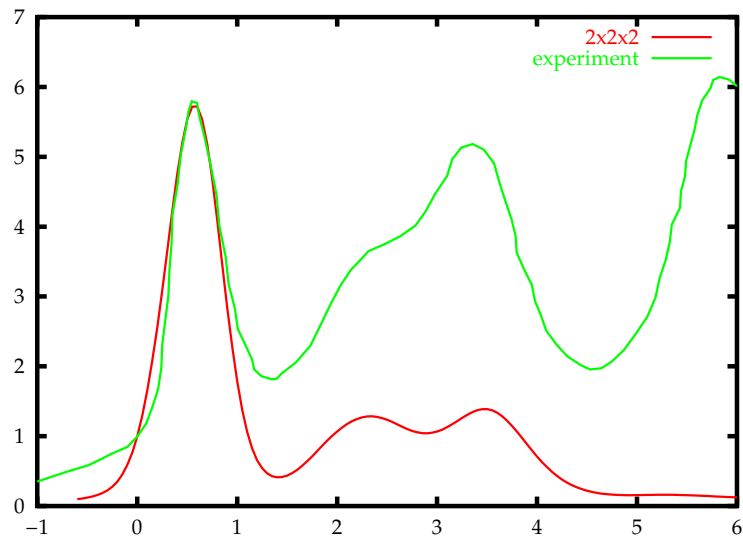


Figure 3.15: Ti- L_3 ELNES of titanium oxide in a $2 \times 2 \times 2$ supercell and the experimental spectrum

3.4 Copper

3.4.1 Copper metal

In the simulation a face centred cubic cell ($Fm\bar{3}m$, space group 225) with lattice parameters of $a = b = c = 3.607 \text{ \AA}$ were used. Computational parameters were 5000 k-points in the IBZ and a cut-off parameter of $R_{mt} * k_{max} = 8.0$.

Figure 3.16 shows that in copper the presence of a core hole influences only the height of the peaks in the ELNES but not their respective positions. The decrease in height of the first peak is much more pronounced, such that for a full core hole the first peak is smaller than the third, whereas in the case of no core hole the first peak is the dominant feature in the ELNES.

From the calculations given in tables 3.4.1 and 3.4.1 the energy levels of the Cu L_2 and L_3 states were extracted. Together with the Fermi level the theoretical edge onset was calculated. The calculated values for the 0.5 partial core hole is very close to the experimental values of 931 eV for the L_2 and 951 eV for the L_3 edge of Cu.

The comparison between experiment and simulation in figure 3.17 gives an almost perfect agreement for the simulation with the half (0.5) core hole.

For the $2 \times 2 \times 2$ supercell lattice parameters of $a = b = 13.552 \text{ \AA}$ and $c = 6.776 \text{ \AA}$ were used.

Figure 3.18 shows the comparison of the copper L_3 edge in copper for the single cell (no and half core hole), the spectrum for a $2 \times 2 \times 2$ supercell with a full core hole and

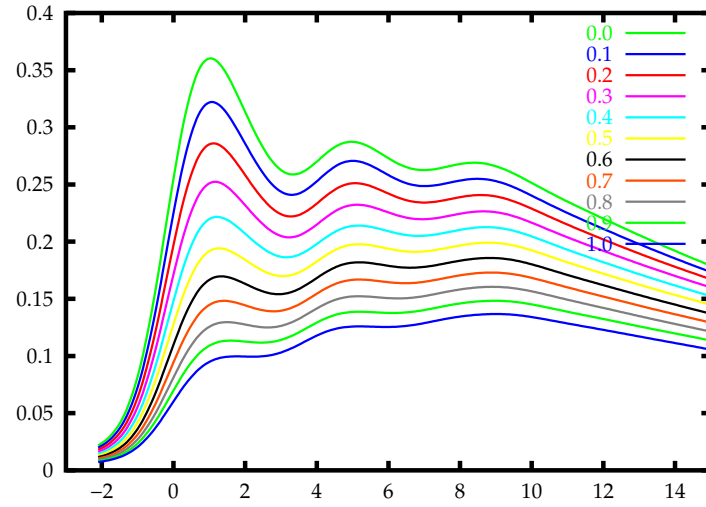


Figure 3.16: Partial core hole in copper Cu L_3 ELNES, varying the core hole from no (0.0) to a full missing electron (1.0)

PCH	$2p_{1/2}$ (Ry)	E_F (Ry)	Edge (Ry)	Edge (eV)
0,0	-66,17040	0,59948	66,77	908,47
0,1	-66,52161	0,57939	67,10	912,98
0,2	-66,87405	0,56069	67,43	917,52
0,3	-67,22791	0,54349	67,77	922,10
0,4	-67,58217	0,52810	68,11	926,71
0,5	-67,93844	0,51405	68,45	931,36
0,6	-68,29685	0,50139	68,80	936,07
0,7	-68,65759	0,48987	69,15	940,82
0,8	-67,02101	0,47928	67,50	918,41
0,9	-69,38656	0,46962	69,86	950,46
1,0	-69,75551	0,46064	70,22	955,36

Table 3.5: Core levels and calculated L_2 edge onset in copper with a partial core hole

PCH	$2p_{3/2}$ (Ry)	E_F (Ry)	Edge (Ry)	Edge (eV)
0,0	-67,67662	0,59948	68,28	928,96
0,1	-68,03307	0,57939	68,61	933,54
0,2	-68,39076	0,56069	68,95	938,15
0,3	-68,74988	0,54349	69,29	942,81
0,4	-69,10940	0,52810	69,64	947,49
0,5	-69,47095	0,51405	69,98	952,22
0,6	-69,83463	0,50139	70,34	956,99
0,7	-70,20066	0,48987	70,69	961,82
0,8	-70,56938	0,47928	71,05	966,69
0,9	-70,94023	0,46962	71,04	966,56
1,0	-71,31453	0,46064	71,40	971,48

Table 3.6: Core levels and calculated L_3 edge onset in copper with a partial core hole

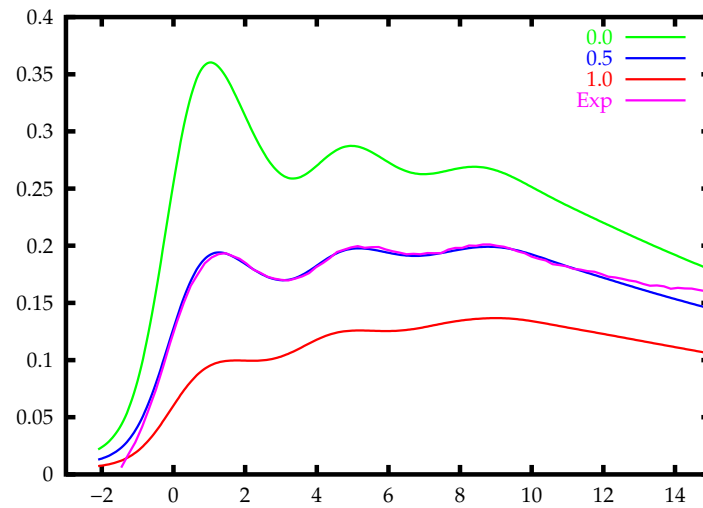


Figure 3.17: Cu L_3 ELNES of copper with no, half and a full core hole, and the experimental spectrum

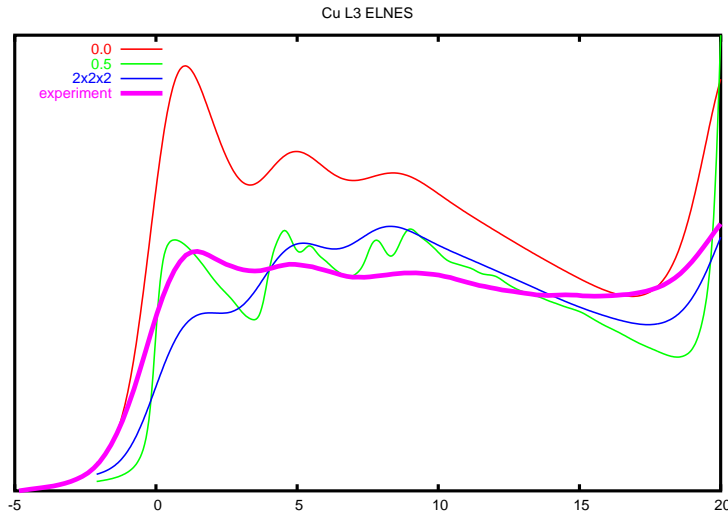


Figure 3.18: ELNES of the Cu L_3 edge in a copper 2x2x2 supercell in comparison with results from the single cell calculation (no and half core hole) and the experiment.

the experimental spectrum. Here we see that the experimental spectrum would be best approximated by mixing the calculated spectra from the single cell with no core hole and the 2x2x2 supercell with a full core hole. A very good approximation is also given by the line from the calculation with half a core hole.

3.4.2 Copper oxide

Copper oxide Cu_2O crystalizes in the cubic space group 224 $Pn\bar{3}m$ with lattice parameters of $a = b = c = 8.064$ Bohr. As calculational parameters 5000 k-points and a cut-off parameter of $R_{mt} * k_{max} = 8.0$ were used.

Figure 3.19 shows the effect of a (partial) core hole on the Cu- L_3 ELNES in copper oxide. By going from no to a full core hole the first peak decreases dramatically in height and shifts from approx. 2.5 eV for no core hole to approx. 5 eV for a full core hole. Comparing with the experiment in figure 3.20 we see that a good agreement between simulation and experiment can be achieved for half a core hole.

For the 2x2x2 supercell lattice parameters of $a = b = c = 16.127$ Bohr were chosen. We see in figure 3.21 that the shape and relative height of the experimental spectrum is best approximated by the simulation with half a core hole in the single cell. The 2x2x2 supercell would exaggerate the first peak with respect to the rest of the spectrum. For computational reasons only the L_3 part of the supercell calculation is shown in fig. 3.21.

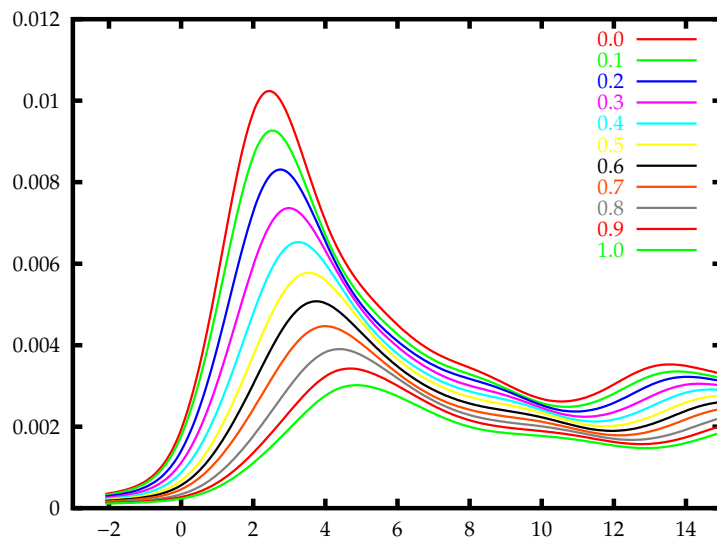


Figure 3.19: Partial core hole in Cu-L₃ ELNES in copper oxide

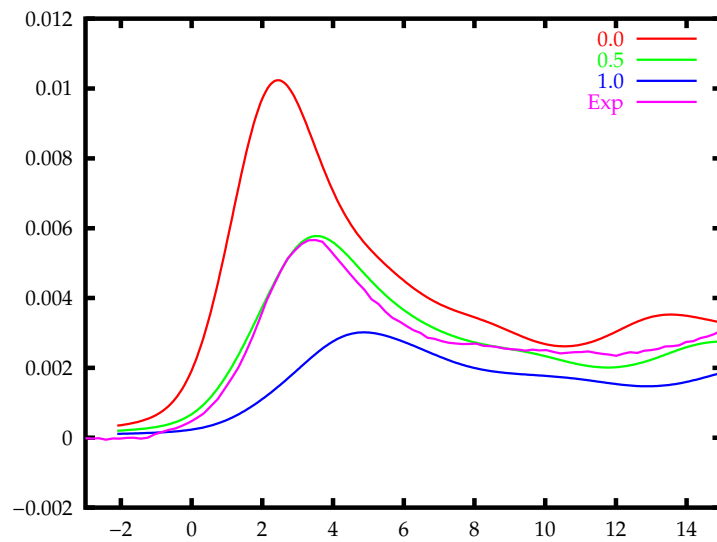


Figure 3.20: Cu-L₃ ELNES of copper oxide with no, half and a full core hole, and the experimental spectrum

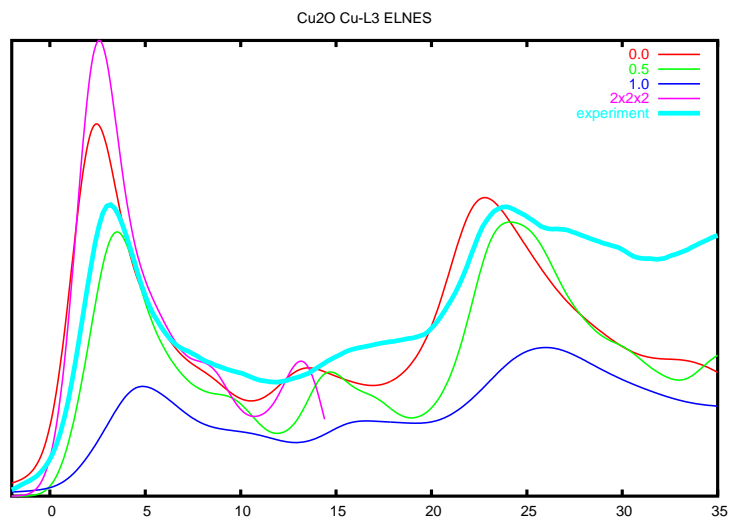


Figure 3.21: Cu L_3 ELNES of copper oxide in a 2x2x2 supercell and comparison with results from the single cell calculation and the experiment

Conclusion

*Facts are more mundane than fantasies,
but a better basis for conclusions.*
Amory Lovins

4 Conclusion

Rez et al. [45] have claimed that whereas in oxides a core hole is needed for the simulation of EELS and XANES, the effect of the core hole can be neglected in metals due to screening by free electrons. We have shown in [29] that for pure copper the core hole is not perfectly screened. In order to take into account this imperfect screening, we have developed the method of the "partial core screening", in which calculations are performed using a partial core hole caused by only a fraction of an electron.

In this thesis we present a systematic study of the effect of the partial core hole in the simulation of metals and oxides of Al, Mg, Ti and Cu and whenever possible also performed a simulation using the "core hole in a supercell" approach.

From the four investigated metals all except magnesium showed best agreement between experiment and simulations for a partial core hole of 0.5 or 0.4. Only in magnesium metal the ground state simulation shows better agreement.

For the oxides the simulations using a core hole generally gives worse results in the simple unit cell using a full core hole. This fact is due to the periodic images of the core hole and thus an artificial core hole – core hole interaction in the simulation. By performing a calculation in a supercell this interaction can be diminished, if not suppressed.

However, the agreement between experiment and simulation – at least for the systems presented in this work – are generally better for the metals than for the oxides. This is due to the fact that the relative peak heights are generally not in good agreement with experiment, and are usually better for the metals.

In contrast to peak heights, the peak positions, i.e. the excitation energies, can be very well reproduced using Slater's transition state (as mentioned in 1.9.4), which is equivalent to a partial core hole of 0.5 electrons.

We have shown that "partial core screening" is a useful concept for the improvement of simulated spectra, but it will never be an accurate description of excited states. As of today there are codes available that implement newer theories that are better suited for the simulation of excited state properties, like GW, TD-DFTE, BSE or Current Density Functional Theory. These are, however not (yet) implemented in the current WIEN2k package.

Thanks

*Art and science have their
meeting point in method.*

Paul Dirac

Angels fly because they take themselves lightly... This sentence always showed up whenever I received an email from my friend and colleague Dieter Kvasnicka. It was he who constantly helped me whenever I had a problem with FORTRAN, regular expressions, or whatever. I thank him for his patience in particular when debugging my code. He still calls me an "experimental programmer"...

A major part of thanks go to Peter Blaha and Karlheinz Schwarz. It was Peter who initiated me into the secrets of the WIEN2k code (I think the first version I stumbled over was some sort of WIEN95) and Karlheinz for giving me the necessary theoretical understanding about solid state theory and DFT.

Not to forget Michel Nelhiebel, for the theoretical derivation of the original EELS formulae, and Pierre Henry Louf for the first version of the telnes code. I want to thank Peter Schattschneider for enabling these two to carry out their work and also for employing my wife in his group. Also an important contribution to this work has come from Kevin Jorissen, who has spent some time with us in Gablitz to develop the theoretical foundation of the TELNES.2 code.

The first ideas of the partial core hole date back to a course on the "theory of metallic bonding" held in Graz in 2000 by Jorge Sofo and organized by Claudia Ambrosch Draxl. I think it was during a late night Grappa session that Claudia said "does it have to be a whole core hole"?

I am grateful to my parents, who have brought me up such that I had the liberty to ponder over thoughts like the ones presented in this work.

In addition I thank my children Joseph André (aged 3 years) and Anne Sophie (aged 20 months) for their patience ...

My final thanks go to my wife Cécile: without her assistance this work would have never been possible – she provided almost all of the experimental data presented in this work.

Bibliography

Bibliography

- [1] <http://nobelprize.org/chemistry/laureates/1998>.
- [2] N. W. Ashcroft and N. D. Mermin. *Festkörperphysik*. Oldenbourg, 2001. ISBN 3486248340.
- [3] O. Krogh Andersen. Linear methods in band theory. *Phys. Rev. B*, 12(8):3060–3083, 1975.
- [4] P. Blaha, K. Schwarz, G Madsen, D. Kvasicka, and J. Luitz. *WIEN2k, An Augmented Plane Wave + Local Orbital Program for Calculating Crystal Properties*. Karlheinz Schwarz, Techn. Universität Wien, Austria, 2001.
- [5] Peter Blaha. *Dissertation*. PhD thesis, TU Wien, 1981.
- [6] Peter Blaha, Karlheinz Schwarz, P. Sorantin, and S.B. Trickey. Full-potential, linealized augmented plane wave programs for crystalline systems. *Computer Physics Communications*, 59:399–415, 1990.
- [7] D. M. Ceperley and B. J. Alder. *Phys. Rev. Lett.*, 45:566, 1980.
- [8] L. Duò, M. Sancrotti, G. Currò, A. Ruocco, S. D'Addato, R. Cosso, P. Unsworth, and P. Weightman. Strong evolution of the p-projected empty density of states in Pd-Al alloys: an $M_{4,5}$ X-ray-absorption-spectroscopy investigation. *Physical Review B*, 47(12):6937–6941, 1993.
- [9] R. Egerton. Electron energy loss spectroscopy. *Physics World*, 47-51, 1996.
- [10] C. Elsässer and S. Köstlmeier. Density-functional modelling of core-hole effects in electron energy-loss near-edge spectra. *Ultramicroscopy*. 2001 Feb;86(3-4):325–37., 86(3-4):325–337, Feb. 2001.
- [11] M. Grioni, M. T. Czyżyk, M. F. de Groot, J. C. Fuggle, and B. E. Watts. Unoccupied electronic states of CuO: An oxygen 1s x-ray absorption spectroscopy investigation. *Physical Review B*, 39(8):4886–4890, 1989.

- [12] M. Grioni, J. F. van Acker, M. T. Czyżyk, and J. C. Fuggle. Unoccupied electronic structure and core-hole effect on the x-ray absorption spectra of Cu_2O . *Physical Review B*, 45(7):3309–3318, 1992.
- [13] K. Guerlin. *Vergleichende Untersuchung der Perowskite Calcium-, Strontium- und Bariumtitanat mit Hilfe der kantennahen Feinstruktur in Elektronenenergieverlustspektren*. Wissenschaft und Technik Verlag, Berlin, 1996.
- [14] J. Hafner. *Quantentheorie. Skriptum*, Technische Universität Wien, 1994.
- [15] P. Hohenberg and Walter Kohn. Inhomogeneous electron gas. *Physical Review*, 136(3B):B864–B871, 1964.
- [16] C. Hébert, J. Luitz, and P. Schattschneider. Improvement of energy loss near edge structure calculation using wien2k. *Micron*, 34(3-5):219–225, 2003.
- [17] C. Hébert, P. Schattschneider, H. Franco, and B. Jouffrey. *Ultramicroscopy*, submitted.
- [18] C. Hébert, P. Schattschneider, J. Luitz, and C. Ambrosch-Draxl. Core loss spectroscopies - a comparison between elnes and xanes. In Y. Ito et al. Y. Azuma, editor, *Proceedings of International Seminar on Photoionization in Atom*, pages 45–50. Kyoto University Press, 2002.
- [19] C. Hébert-Souche, P-H Louf, P. Blaha, M. Nelhiebel, J. Luitz, P. Schattschneider, K. Schwarz, and B. Jouffrey. The orientation dependent simulation of ELNES. *Ultramicroscopy*, 83(1-2):9–16, 2000.
- [20] K. Jorissen. *ELNES Code Developers' Guide*.
- [21] K. Jorissen, J. Luitz, and C. Hébert. A program for the calculation of energy loss near edge structure: the new and improved telnes.2 code. In Gerald Kothleitner, editor, *Advanced Data Generated with Electrons*. D. Müller, TU Graz.
- [22] K. Jorissen, J. Luitz, and C. Hébert. A program for the calculation of energy loss near edge structure: the new and improved telnes.2 code. *Ultramicroscopy*, submitted.
- [23] Walter Kohn and L. J. Sham. Self-consistent equations including exchange and correlation effects. *Physical Review*, 140(4A):A1133–A1138, 1965.
- [24] K. Kopitzki. *Einführung in die Festkörperphysik*. Teubner, Stuttgart, 1986.
- [25] K. Kurki-Suonio. *Israel J. Chem*, 16:115, 1977.
- [26] R. D. Leapman, P. L. Fejes, and J. Silcox. Orientation dependence of core edges from anisotropic materials determined by inelastic scattering of fast electrons. *Physical Review B*, 28(5):2361–2373, 1983.

- [27] P. Lerch, T. Jarlborg, V. Codazzi, G. Loupiaz, and A. M. Flank. X-ray-absorption spectroscopy in CoSi_2 and NiSi_2 : experiment and theory. *Physical Review B*, 45(20):11481–90, 1992.
- [28] K. Lie, R. Brydson, and H. Davock. Band structure of TiB_2 : Orientation-dependent EELS near-edge fine structure and the effect of the core hole at the B K edge. *Physical Review B*, 59(9):5361–5367, 1999.
- [29] J. Luitz, C. Hébert, P. Schattschneider, P. Blaha, K. Schwarz., and B. Jouffrey. Partial core hole screening in the Cu L3 edge. *Eur.Phys.J.*, 2001.
- [30] O. Madelung. *Festkörperphysik I*. Teubner, Stuttgart, 1972.
- [31] G. K. H. Madsen, P. Blaha, K. Schwarz, E. Sjöstedt, and L. Nordström. *Phys. Rev. B* 64, 64(195134), 2001.
- [32] P. Mohn. Interpretation der röntgenemissionsspektren der intermetallischen verbindungen FeAl, CoAl, NiAl. Master's thesis, TU Wien, 1981.
- [33] David A. Muller, David J. Singh, and John Silcox. Connections between the electron-energy-loss spectra, the local electronic structure, and the physical properties of a material: A study of nickel aluminium alloys. *Physical Review B*, 57(14):8181–8202, 1998.
- [34] J. E. Müller and J. W. Wilkins. Band-structure approach to the x-ray spectra of metals. *Phys. Rev. B*, 29:4331–4348, 1984.
- [35] A. Neckel, P. Rastl, R. Eibler, P. Weinberger, and K. Schwarz. Result of self-consistent band-structure calculations for ScN, ScO, TiC, TiN, TiO VC VN and VO. *Journal of Physics C*, 9:579–592, 1976.
- [36] A. Neckel, K. Schwarz, R. Eibler, P. Rastl, and P. Weinberger. *Microchim. Acta*, Suppl. 6, 1975.
- [37] M. Nelhiebel, P.-H. Louf, P. Schattschneider, P. Blaha, K. Schwarz, and B. Jouffrey. Theory of orientation sensitive near-edge fine structure core-level spectroscopy. *Physical Review B*, 59(20):12807–12814, 1999.
- [38] M. Nelhiebel, P-H Louf, P. Schattschneider, P. Blaha, K. Schwarz, and B. Jouffrey. Theory of orientation sensitive near-edge fine structure core-level spectroscopy. *Physical Review B*, 59(20):12807–12814, 1999.
- [39] P. Novak. private communication.
- [40] Ernst A. Nusterer. *Dissertation*. PhD thesis, TU Wien, 1996.
- [41] J. P. Perdew, K. Burke, and M. Ernzerhof. *Phys. Rev. Lett.*, 77:3865, 1996.

- [42] John P. Perdew and Yue Wang. Accurate and simple analytic representation of the electro-gas correlation energy. *Physical Review B*, 45(23):13244–13249, 1992.
- [43] P. L. Potapov, K. Jorissen, and D. Schryvers. Effect of charge transfer on EELS integrated cross sections in Mn and Ti oxides. *Physical Review B*, 70:045106–1 – 045106–10, 2004.
- [44] K. Rahkonen and K. Krause. *Atomic Data and Nuclear Data Tables*, 14(2), 1974.
- [45] Peter Rez, J. Bruley, P. Brohan, M. Payne, and L. A. J. Garvie. Review of methods for calculating near edge structure. *Ultramicroscopy*, 59:159–167, 1995.
- [46] P. Schattschneider. Electron energy loss spectrometry. Skriptum, Technische Universität Wien, 1995.
- [47] P. Schattschneider, C. Hébert, H. Franco, and B. Jouffrey. *Phys. Rev. B*, in press.
- [48] P. Schattschneider, S. Rubino, C. Hébert, J. Ruz, and P. Novak. *Ultramicroscopy*, submitted.
- [49] Peter Schattschneider. *Fundamentals of Inelastic Electron Scattering*. Springer-Verlag, Wien, New York, 1986.
- [50] K. Schwarz. Dft calculations of solids with LAPW and WIEN2k. *J. Solid State Chem.*, 176:319–328, 2003.
- [51] K. Schwarz and P. Blaha. Solid state calculations using WIEN2k. *Comp. Mat. Sci.*, 28:259–273, 2003.
- [52] D. J. Singh. *Phys. Rev. B*, 43:6388, 1991.
- [53] David Singh. *Plane waves, pseudopotentials and the LAPW method*. Kluwer Academic, 1994.
- [54] David J. Singh. *Planewaves, Pseudopotentials and the LAPW Method*. Kluwer Academic Publishers, Boston Dordrecht London, 1994.
- [55] E. Sjöstedt, L. Nordström, and D. J. Singh. An alternative way of linearizing the augmented-plane-wave method. *Phys. Rev. B*, 1999.
- [56] E. Sjöstedt, L. Nordström, and D. J. Singh. *Solid State Commun.*, 114, 15, 2000.

- [57] J. C. Slater. Wave functions in a periodic potential. *Phys. Rev.*, 51:846–851, 1937.
- [58] John C. Slater. *The Self-consistent Field for Molecules and Solids*, volume 4, chapter The Dependence of Total Energy on Occupation Numbers, pages 35–55. McGraw-Hill, 1980.
- [59] P. J. W. Weijts, M. T. Czyżyk, J. F. van Acker, W. Speier, G. van der Laan, K. H. J. Buschow, G. Wiech, and J. C. Fuggle. Core-hole effects in the x-ray absorption spectra of transition-metal silicides. *Physical Review B*, 41(17):11899–11910, June 1990.

Curriculum Vitae

Joachim Luitz

Wohlmuthgasse 18, A-3003 Gablitz
Manoir du Serpolet, F-63430 Pont-du-Château

geboren am 11. 1. 1967 in Wien
Österreichischer Staatsbürger

verheiratet mit Dr. Cécile Hébert seit 10.02.2001
Sohn Joseph André geb. 27.5.2003
Tochter Anne Sophie geb. 29.8.2004

Ausbildung und beruflicher Werdegang

- 1981-1986 Höhere Technische Bundes Lehr- und Versuchsanstalt für chemische Industrie, Wien 1170 ("Rosensteingasse"); Abteilung für Technische Chemie; Matura im Mai 1986
- 1986-1988 Wissenschaftlicher Mitarbeiter am Institut für Limnologie der Universität Wien, Forschungsschwerpunkt: Gewässeranalytik
- 1988 Wissenschaftlicher Mitarbeiter bei Greenpeace Deutschland e.V., Schwerpunkt: Analytik von Luftschadstoffen
- 1989 Präsenzdienst beim Österreichischen Bundesheer
- 1989-1994 Erster Studienabschnitt des Chemiestudiums an der Universität Wien
- 1991-1992 Speziallehrgang für Technischen Umweltschutz
Höhere Technische Bundes-Lehr- und Versuchsanstalt für chemische Industrie, Wien 1170 ("Rosensteingasse")
- 1994-1996 Zweiter Studienabschnitt des Studiums der Technischen Chemie an der Technischen Universität Wien, Fachrichtung Physikalische Chemie, Spon- sion im September 1996
- 1996-1997 Wissenschaftlicher Angestellter bei Prof. Blaha, Inst. f. Physikalische Chemie, TU Wien;
Schwerpunkt: Dichtefunktional-Methoden, "Linearized Augmented Plane Wave Methods" (LAPW); Weiterentwicklung des Programmpakets WIEN97; Simulation von Core-Level Spektren, sowie graphische Benutzeroberfläche
- 1997-2000 Wissenschaftlicher Angestellter im Rahmen des Sonderforschungsbereichs "AURORA", Universität Wien; Schwerpunkt: Weiterentwicklung des Programmpakets WIEN2k, insbesondere im Bereich der Parallelisierung
- 1997- Geschäftsführer der Firma Dipl. Ing. Joachim Luitz KEG – Informationstechnologie, Internet, Netzwerke und Multimedia
- 1999- Obmann des Vereins der Freunde der Festkörperphysik und -chemie
- 2000- Konzessionsprüfung und Gewerbeberechtigung für Technische Büros für technische Chemie

Informationstechnologie & Multimedia

Aufbau von Computernetzwerken, Installation und Konfiguration von Servern. Betrieb eigener Web- und Mailserver unter Linux. Erstellung von Software: wissenschaftliche Software (Coautor von WIEN2k mit weltweit über 900 Benutzergruppen), Web-Interfaces und Benutzeroberflächen (w2web, tem2web, weather2web, vinothek, wienbox, tkncc), u.a. Seit 1996 hauptverantwortlich für die Konzeption und Realisierung zahlreicher Internet-Präsentationen. Darunter Kultur-Projekte wie "Austrian Music Network", Internationales Kammermusikfestival "Allegro Vivo", "Neue Oper Wien", "Johann Strauß Jahr 1999", unter anderem auch die Homepage der Marktgemeinde Gablitz (mit Meßdateninterface zur bestehenden Wetterstation), oder im technischen Bereich z.B. für die Universitäre Service-Einrichtung für Transmissionselektronenmikroskopie der TU Wien (USTEM) oder das EU-Projekt "EXC!TiNG".

Umweltschutz

- 1989-1997 Mitglied der NÖ Berg- und Naturwacht
- 1992-1996 Leiter der Sondereinsatzgruppe Gewässerschutz der NÖ Berg- und Naturwacht
- Preisträger beim NÖ Umweltpreis 1990 und beim Hans-Zettel Preis 1991
- 1992- Beeidetes Umweltschutzorgan des Landes Niederösterreich
- 1992 "Arbeitskreis Umwelttechnik" im Rahmen des Speziallehrgangs für Technischen Umweltschutz an der Rosensteingasse; damit 2. Preis bei "NÖ Umweltpreis" mit dem Projekt "Gablitz".
- 2000- Geschäftsführer des Technischen Büros für Technische Chemie Dipl. Ing. Joachim Luitz KEG

Musik

- 1973-1981 Violoncello: Musikhochschule Wien, Vorbereitungsklasse
- 1980-1981 Gitarre: Akademisches Gymnasium
- 1981 Trompete: Konservatorium der Stadt Wien
- 1981- Klavier im Selbststudium

Seit 1981 zahlreiche Kompositionen für unterschiedliche Besetzungen. Öffentliche Uraufführungen u.a. durch die Österr. Gesellschaft für zeitgenössische Musik und mit namhaften Interpreten. Selbst öffentliche Auftritte als Interpret (Gesang, Klavier und/oder Gitarre), bisher 2 CD Produktionen eigener Lieder (mit Texten von Bernhard Schaffer)

Austrian Music Network

"Austrian Music Network - www.music.at" ist ein eingetragenes Markenzeichen. Unter diesem Namen werden seit 1997 zahlreiche Musiker und Institutionen multimedial beraten und betreut. Das Austrian Music Network hat sich als Ziel gesetzt das führende österreichische Portal für klassische und zeitgenössische Musik zu werden. Seit 2001 ist das Austrian Music Network auch eingetragenes Platten(CD)-Label.

Wissenschaft und Forschung

Seit 1995 Mitarbeit an der Forschung im Bereich der Festkörperphysik und -chemie. Schwerpunkt sind Simulationen von Core-Loss Spektren (mittels Röntgen oder Elektronenenergieverlust) und die Weiterentwicklung des Programmpakets WIEN2k (vormals WIEN97 bzw. WIEN95), das auf der vom Nobelpreisträger Walter Kohn entdeckten Dichtefunktionaltheorie (DFT) beruht.

Seit 1996 Vortragender bei den jährlich stattfindenden WIEN97 bzw. WIEN2k Workshops (Wien; State College, USA; Kyoto, Japan); 1998-2002 und 2006 Mithilfe bei der Organisation dieser Workshops

22.6.1998 – 4.7.1998 Gastvortragender beim "Workshop on the physics of the electronic behaviour in the core region: all-electron LAPW electronic structure calculations" am ICTP - The Abdus Salam International Centre for Theoretical Physics, Trieste, Italy.

Seit Dezember 1999 Obmann des Vereins der Freunde der Festkörperphysik und -chemie.

14.–17.1.2001 Verantwortlicher Organisator der "International Conference on Applied Density Functional Theory 2001" an der TU Wien unter Ehrenvorsitz von Prof. Walter Kohn.

21.–23. April 2006 Verantwortlicher Organisator der International Conference on Density Functional Theory (DFT) and Transmission Electron Microscopy (TEM) "DFTEM 2006 – bringing together two communities" in Wien.

Mitgliedschaften

GÖCH – Gesellschaft österr. Chemiker

WKO – Wirtschaftskammer Österreich

Verein der Freunde der Festkörperphysik und -chemie

AKM – Autoren, Komponisten und Musikverleger

GLOBArt – Connecting worlds of arts and sciences

Sprachen

Deutsch: Muttersprache

Englisch: Perfektion in Wort und Schrift

Französisch: Arbeitskenntnisse

Spanisch: Anfänger

Sonstiges

Führerschein: A,B,C,E,F,G

Internationales Küstenpatent und Seefunkzeugnis

Seit 2001 Laienrichter am Landesgericht St. Pölten für Arbeits- und Sozialrecht

Publikationen

- [14] **DFTEM2006 – bringing together two communities**
 Joachim Luitz et al. (Hrsg)
 Proceedings of the International Conference on Density Functional Theory and Transmission Electron Microscopy, April 21-23, 2006, Vienna/Austria Editio Amici, ISBN: 3-902548-00-2
- [13] **A program for the calculation of Energy Loss Near Edge Structure. The new and improved TELNES.2 Code**
 K. Jorissen, J. Luitz and C. Hébert
 in "Enhanced Data Generated with Electrons", D. Müller (hrsg.), TU Graz, Gerald Kothleitner, 2005
 also submitted to Ultramicroscopy
- [12] **Musikhandbuch für Österreich** : Datensammlung zum Musikleben in Österreich
 hrsg. von d. Österreichischen Gesellschaft für Musik. Generiert aus d. Datenbank d. Austrian Music Networks www.music.at von Joachim Luitz... Stand 24. Juni 2003. Musikverlag Doblinger, Wien. ISBN 3 900695 58 X
- [11] **Improvement of energy loss near edge structure calculations using WIEN2k**
 C. Hébert, J. Luitz, P. Schattschneider
 Micron 34, 219-225, 2003
- [10] **Itinerant metamagnetism and possible spin transition** in LaCoO₃ by temperature/hole doping
 P. Ravindran, H. Fjellvag, A. Kjekshus, P. Blaha, K. Schwarz and J. Luitz
 J. Appl. Phys. 91, 291 (2002)
- [9] **WIEN2k: An Augmented Plane Wave plus Local Orbitals Program for Calculating Crystal Properties**
 P. Blaha, K. Schwarz, G. Madsen, D. Kvasnicka and J. Luitz
 TU Wien, 2001 (ISBN 3-9501031-1-2)
- [8] **Partial core hole screening in the Cu L3 edge**
 J. Luitz, M. Maier, C. Hébert, P. Schattschneider, P. Blaha, K. Schwarz and B. Jouffrey
 Eur. Phys. J. B21, 363 (2001)
- [7] **On Using Spider to Examine and Debug Real-World Data-Parallel Applications**
 T. Fahringer, K. Sowa, J. Luitz, H. Moritsch
 6th International Conference on Parallel Computing Technologies (Pact-2001)
 Lecture Notes in Computer Science, Springer
- [6] **Development and Performance Analysis of Real-World Applications** for Distributed and Parallel Architectures
 T. Fahringer, P. Blaha, A. Hössinger, J. Luitz, E. Mehofer, H. Moritsch, and B. Scholz
 Concurrency and Computation: Practice and Experience (Ed. Geoffrey Fox), 13(10): 841-868 (2001)
- [5] **Electronic structure and chemical bonding effects** upon the bcc to Omega phase transition: Ab initio study of Y, Zr, Nb, and Mo
 G. B. Grad, P. Blaha, J. Luitz, K. Schwarz, A. Fernandez Guillermet, S. J. Sferco
 Phys. Rev. B62, 12743 (2000)

[4] **The orientation-dependent simulation of ELNES**

C. Hebert-Souche, P.-H. Louf, P. Blaha, M. Nelhiebel, J. Luitz, P. Schattschneider, K. Schwarz, B. Jouffrey
Ultramicroscopy, 83, 9-16 (2000)

[3] **Calculations of electric field gradients in solids: How theory can complement experiment**

P. Blaha, K. Schwarz, W. Faber and J. Luitz
Hyperfine Int. 126, 389 (2000)

[2] **WIEN97, A Full Potential Linearized Augmented Plane Wave Package for Calculating Crystal Properties**

P. Blaha, K. Schwarz and J. Luitz
Karlheinz Schwarz, Techn. Univ. Wien, Vienna 1999 (ISBN 3-9501031-0-4)

[1] **XAFS: A Unique Tool to Study the Intercalation Process**

G. Ouvrard, S. Lemaux, Z. WU, P. Gressier, J. Luitz
Mol Cryst. Liq. Cryst 311 (1998)